Hawaii National Marine Renewable Energy Center (HINMREC)

U.S. Department of Energy Award Number: DE-FG36-08GO18180

Task 5: Wave Energy Conversion Device Performance

WEC Ocean Testing: Performance Model Verification, Progress Report 2

Prepared by:
DNV GL Energy

Prepared for:
Hawaii Natural Energy Institute, University of Hawaii

June 2016

HNEI
Hawai'i Natural Energy Institute
University of Hawai'i at Mānoa

HAWAII NATIONAL MARINE RENEWABLE ENERGY CENTER – WEC OCEAN TESTING

WEC Performance Model Verification – Progress Report #2

Hawaii Natural Energy Institute (HNEI)

Report No.: 702053-USSD-T-05, Rev. B
Date: 07 June 2016

IMPORTANT NOTICE AND DISCLAIMER

1. This document is intended for the sole use of the Client as detailed on the front page of this document to whom the document is addressed and who has entered into a written agreement with the DNV GL entity issuing this document ("DNV GL"). To the extent permitted by law, neither DNV GL nor any group company (the "Group") assumes any responsibility whether in contract, tort including without limitation negligence, or otherwise howsoever, to third parties (being persons other than the Client), and no company in the Group other than DNV GL shall be liable for any loss or damage whatsoever suffered by virtue of any act, omission or default (whether arising by negligence or otherwise) by DNV GL, the Group or any of its or their servants, subcontractors or agents. This document must be read in its entirety and is subject to any assumptions and qualifications expressed therein as well as in any other relevant communications in connection with it. This document may contain detailed technical data which is intended for use only by persons possessing requisite expertise in its subject matter.

2. This document is protected by copyright and may only be reproduced and circulated in accordance with the Document Classification and associated conditions stipulated or referred to in this document and/or in DNV GL's written agreement with the Client. No part of this document may be disclosed in any public offering memorandum, prospectus or stock exchange listing, circular or announcement without the express and prior written consent of DNV GL. A Document Classification permitting the Client to redistribute this document shall not thereby imply that DNV GL has any liability to any recipient other than the Client.

3. This document has been produced from information relating to dates and periods referred to in this document. This document does not imply that any information is not subject to change. Except and to the extent that checking or verification of information or data is expressly agreed within the written scope of its services, DNV GL shall not be responsible in any way in connection with erroneous information or data provided to it by the Client or any third party, or for the effects of any such erroneous information or data whether or not contained or referred to in this document.

4. Any wind or energy forecasts estimates or predictions are subject to factors not all of which are within the scope of the probability and uncertainties contained or referred to in this document and nothing in this document guarantees any particular wind speed or energy output.

KEY TO DOCUMENT CLASSIFICATION

Strictly Confidential	:	For disclosure only to named individuals within the Client's organisation.
Private and Confidential	:	For disclosure only to individuals directly concerned with the subject matter of the document within the Client's organisation.
Commercial in Confidence	:	Not to be disclosed outside the Client's organisation.
DNV GL only	:	Not to be disclosed to non-DNV GL staff
Client's Discretion	:	Distribution for information only at the discretion of the Client (subject to the above Important Notice and Disclaimer and the terms of DNV GL's written agreement with the Client).
Published	:	Available for information only to the general public (subject to the above Important Notice and Disclaimer).

Project name:	Hawaii National Marine Renewable Energy Center – WEC Ocean Testing	DNV GL Energy
Report title:	WEC Performance Model Verification – Progress Report #2	Renewables Advisory Americas
		9665 Chesapeake Drive
		Suite 435
Customer:	Hawaii Natural Energy Institute (HNEI)	San Diego
Contact person:	Luis Vega	CA 92123
Date of issue:	07 June 2016	USA
Project No.:	702053	Tel: +44 117 972 9900
Report No.:	702053-USSD-T-05, Rev. B	Registered in America No. 94-3402236

Prepared by: Verified by: Approved by:

_____

Steve Parkinson
Engineer

Armando Alexandre
Engineer

[Name]
[title]

[Name]
[title]

[Name]
[title]

[Name]
[title]

☐ Strictly Confidential
☐ Private and Confidential
☐ Commercial in Confidence
☐ DNV GL only
☒ Client's Discretion
☐ Published

Keywords:
Performance, Loading, Verification

Reference to part of this report which may lead to misinterpretation is not permissible.

Rev. No.	Date	Reason for Issue	Prepared by	Verified by	Approved by
0	09/05/2016	First issue	Steve Parkinson	Armando Alexandre	
1	07/06/2016	Revision following comments	Steve Parkinson	Armando Alexandre	

Table of contents

Appendices

1 INTRODUCTION

This technical note is issued to the Research Corporation of the University of Hawaii (RCUH or the "Customer") pursuant to a written Agreement for Services effective 14 March 2013 and RCUH Purchase order #Z10027978 /1/ as well as the subsequent amendment to the agreement /2/. The Customer has requested that Garrad Hassan America, Inc. (DNV GL) perform services relating to the establishment of a wave energy test centre for the University of Hawaii, Hawaii Natural Energy Institute (UH HNEI). UH HNEI's Hawaii National Marine Renewable Energy Center (HINMREC), under funding fom the U.S. Department of Energy (DOE) is working in collaboration with the U.S. Navy to develop the Wave Energy Test Site (WETS or the "Project") located at the U.S. Marine Corps Base Hawaii – Kanehoe (MCBH-K) in Oahu, Hawaii.

The project consists of three main components /1/:

1. Documentation of test protocols and support to the testing program

2. Provision of data for verification of Wave Energy Converter (WEC) performance models

3. Provision of data for verification of WEC array models

The present technical note forms part of the *second* project component.

As part the service agreement /1/, the scope of the second component of the project is to use DNV GL's WEC performance and loading analysis tool WaveDyn to assist with the verification of HNEI's WEC performance model. WaveDyn has been subjected to a range of validation exercises and wave developed specifically for WECs. The tool allows for flexible, multi-body modelling of a wide range of WEC concepts in time domain simulations and couples loading from critical sources including hydrodynamics, power take off (PTO), and moorings.

Initially it was intended that HNEI would supply outputs from their own performance models for a series of real WEC devices being tested at the WETS site and DNV GL would generate independent models and simulations for comparison. However, due to the lack of availability of data relating to the devices being tested at WETS and following discussions with HNEI, it has been agreed /4/ that DNV GL will instead simulate a range of *generic* WEC models in conditions representative of the WETS site in order to provide a database of loads and power extraction for later use by HNEI.

An advantage of basing this work on a range of generic WEC devices is that the definition of each model can be chosen to clearly demonstrate a variety of physical phenomena that are important to capture by any numerical model. Also, the chosen models can be based on other previous physical or numerical validation work (see /6/ and /10/), which is beneficial for cross-reference of results.

Furthermore, it has been agreed between DNV GL and HNEI /4/ that the technical support to the testing programme detailed in /1/ under deliverables 5.1 and 5.2 would be substituted with further verification data for HNEI's numerical models. This will increase confidence in the numerical predictions calculated by HNEI and thus enhance understanding of the WECs behaviour installed at WETS.

Therefore, the present phase of work (provision of data for verification of WEC Performance models) is associated with five deliverables:

1. WEC performance model verification progress report # 1 – Define rounded cylinder single-body point absorber geometry/size most appropriate for WETS conditions and to inform scaling of geometries in Deliverables 2-5.

2. Testing support progress report #1 – WaveDyn modeling of rounded cylinder single-body point absorber.

3. WEC performance model verification progress report #2 – WaveDyn modeling of flat-profile, single-body point absorber (at same optimized scale as found for rounded cylinder in 1)

4. Testing support progress report #2 – WaveDym modeling of 2-body point absorber based on Department of Energy reference model geometry (at same optimized size found for WETS during 1)

5. WEC performance model verification final report – Assess the extreme loads of a WEC model test case wave energy converter using various methods.

The first two deliverables were reported in /6/ and /7/, the present scope of work will consider the second generic WEC model: *a rounded circular plate single-body point absorber*.

The present technical note refers to the *third* deliverable for this phase and documents the progress that has been made on the analysis of the flat cylinder single-body point absorber. Detailed performance and loading results are presented for the selected scale and water depth. All numerical simulations were performed at model scale and the results included in this technical note at full scale using Froude Scaling laws. Flow solver inputs have been generated to describe the flat-plate hydrodynamics. Results have been derived for both normal and extreme conditions. The normal environmental conditions are based on a range of sea states and a subset of which is representative of the WETS site. Extreme conditions are based on the analysis of on-site measured data sets /7/.

Section 2 describes the setup of the numerical model necessary for this work. The corresponding results in normal operational and extreme sea states are given in Section 3. Finally, some concluding remarks are given in Section 4. All input and output files will be supplied to HNEI to facilitate further verification exercises (via an agreed medium).

2 MODEL SETUP AND OUTPUTS

The simulations in this report have been conducted using a point absorber type WEC. The WEC geometry and the WaveDyn model used for numerical simulation in the present study is depicted in Figure 2-1 and Figure 2-2 respectively.
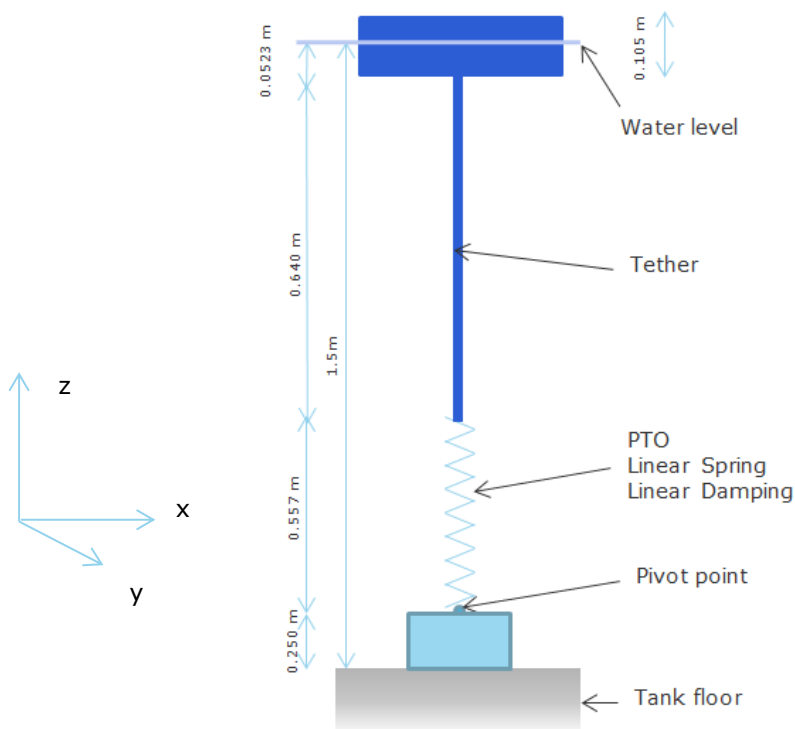
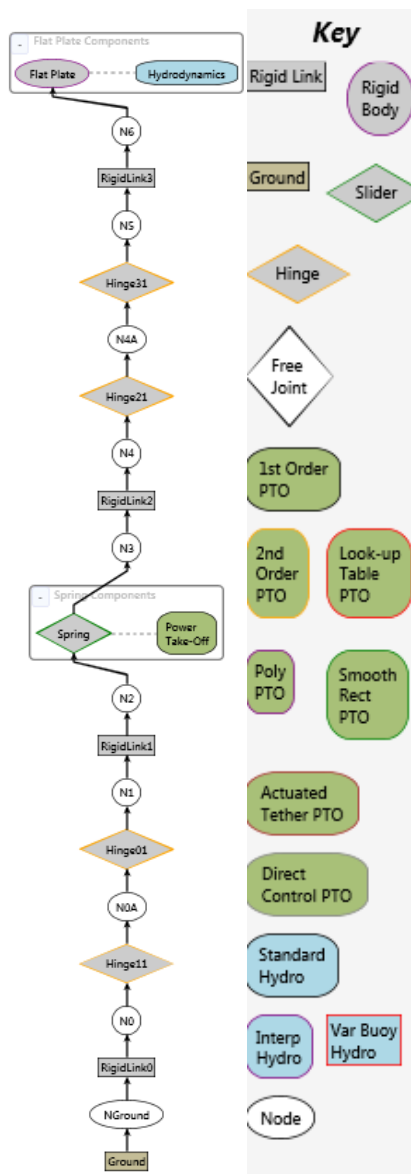**Figure 2-1 Schematic of generic flat-plate WEC device moored to the tank floor.**

Figure 2-2 WaveDyn model schematic.

The point absorber model used in the numerical simulations is similar to that described in /7/. Attempts have been made to preserve the resonant frequency of the system, the mass of the float and the pre-load tension in the tether. The following changes have been made:

1. The buoy has been replaced by a flat-plate with a shallow draft and of the same mass M=43.2 kg. The flat plate is a thin walled body comprising a cylindrical shell and two disks on the top and the bottom which seals the interior. The diameter is 1.05 m and height is 0.105 m. These dimensions were chosen as they represent the widest and flattest WEC point absorber geometry currently being considered and therefore provides a good contrast to the geometry considered in /7/. The mass is uniformly distributed throughout the body such that the center of mass is coincident with the geometric center of the body. The moment of inertia with respect to the center of mass of the body is given by I_{xx}=3.22, I_{yy}= 3.22 and I_{zz}=6.45 kg m^2. The coordinate system is defined in Figure 2-1 for reference.

2. The length of the structural component "rigid link 2" of the WEC in the WaveDyn file was increased to 0.640 m. An increase in the link length is required to ensure the correct draft of the flat-plate in the WaveDyn model (match the hydrodynamic model).

3. The flow solver (WAMIT) simulations were re-run to update the hydrodynamic coefficients for the flat-plate geometry. The draft of the plate is taken as 0.0523 m such that the vertical position of the centre of mass is coincident with the water level. The flat plate is taken to be symmetric around the water level. The pre-load on the spring results in an increase in the draft of the flat-plate. Given the water plane area of the flat-plate is large, it is found that the change in draft is negligible (≈ 2.12 mm). The additional increase in pre-load also results in an increase in the displaced mass from 44.9 kg to 46.9 kg which is considered small.

All simulations were conducted at model scale. However, the outputs have been reported as full-scale values using the Froude scaling set out in /6/. The ratio between lengths in the new point absorber numerical model and the desired 'full-scale' device is 1:40 and so a scale factor of k=40 is used to transform outputs from model to 'full-scale'.

The WEC response to extreme and normal operational conditions are described by the following outputs:

1. The 'Flat-Plate-ST-Kinematics' (i.e. the motions of the flat-plate in global space). These quantities will be reported at the attachment point between the flat-plate and the rigid link connecting the body to the PTO:

    a. Global Surge ϕ_x

    b. Global Sway ϕ_y

    c. Global Heave ϕ_z

    d. Global Roll ϕ_{Rx}

    e. Global Pitch ϕ_{Ry}

2. The 'Total System Power Take-Off (PTO) Performance' (power absorbed by the damper before any losses in the electrical system are taken into account):

    a. PTO Power Output ϕ_P

3. The 'Spring-By-Freedom-PTO' (i.e. tether-related variables). These quantities report the PTO spring forces and displacement.

a. Joint Freedom Displacements ϕ_d

b. Applied Force ϕ_F

Note that none of the simulations took into account quadratic viscous forces, which are difficult to characterise accurately for these type of models. In future studies, CFD simulations of the flat plate will be conducted using Computational Fluid Dynamics which will account for quadratic viscous drag. When modelling energetic and extreme conditions, viscous forces are likely to become important. However, results are presented here using the linear hydrodynamic formulation so that verification exercises with equivalent formulations may be easily performed.

Prior to running simulations a calm water test was conducted to check the equilibrium position of the flat-plate on the still water surface. A calm water test is simulated by setting the height of all incoming waves to zero such that the flat-plate naturally reaches its equilibrium position during a time domain simulation. It was found that the initial position of the flat-plate at the beginning of the simulation and the rest location following the calm water test was the same.

2.1 **PTO setting**

For a single body point absorber operating only in heave with constant linear PTO the resonant angular frequency ω_n can be calculated. The resonant frequency is dependent on the mass and stiffness of the total system. The total stiffness in heave is a function of the PTO spring stiffness k_m and the hydrostatic stiffness of the round-plate k_{hs}. The total system mass in heave is a function of the mass of the flat-plate M and the added mass m_r. Note that the added mass is frequency dependent but it has an asymptotic behaviour for higher frequency values which is used in calculations, see Figure 2-3. An approximation normally used for calculating the resonance frequency is to use the value of the added mass at infinite frequency. The equation used to calculate the angular frequency (in rad/s) at which resonance in uncoupled heave motion occurs, is given by

$$\omega_n = \sqrt{\frac{k_{hs} + k_m}{M + m_r(\omega_n)}} \tag{1}$$

At model scale $K_{hs} = 8.43 \times 10^3$ N/m, $k_m = 66.3$ N/m, $m_r = 195$ kg, and $M = 43.2$ kg. This results in a resonant angular frequency at full-scale of 0.932 rad/s.

Assuming motion only in heave, the optimal PTO damping can be calculated for the resonant angular frequency in heave ω_n. Tuning of the damping is achieved when the following is satisfied

$$\gamma_d = b_{33} \tag{2}$$

where $b_{33}(\omega_n)$ is the hydrodynamic radiation damping in heave due to heave motion of the flat-plate at an angular frequency ω_n. For ω_n=0.932 rad/s, the radiation damping is found to be b_{33} =577 Ns/m. This yields an optimal damping of γ_d=577 Ns/m.

It should be noted that the above analysis is only valid for a relatively simplistic case where the point absorber operates solely in heave. Additional degrees of freedom may influence the resonant frequencies of the WEC.
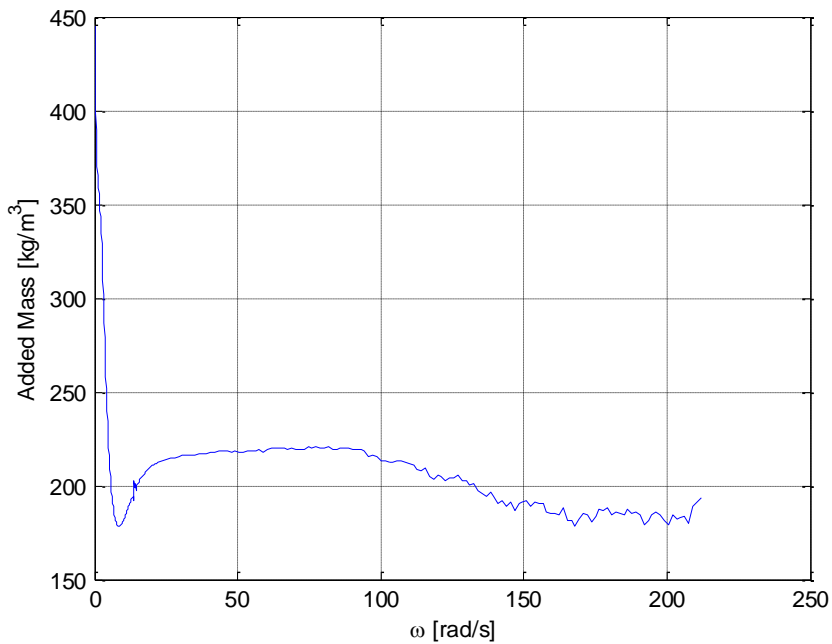
Figure 2-3 Added mass of flat plate in heave motion.

Table 2-1 Main parameters describing the flat-plate point absorber

Parameter	Model scale	Full-scale
Flat-plate definition		
Water depth [m]	1.5	60
Draft [m]	0.0523	2.09
Diameter [m]	1.05	41.8
Mass [kg]	43.2	2.76×10^6
PTO definition		
Damping [Ns/m]	37.7	3.81×10^5
Stiffness [N/m]	66.3	1.06×10^5
Pre-load [N]	35.8	4.59×10^5

3 RESULTS

Time domain simulations of the WEC model described in Section 2 have been conducted in WaveDyn. The environmental conditions are based on numerical and measured data sets obtained for the WETS site and were described in a previous technical note /7/. Appendix A summarises the different environmental conditions used in the WEC simulations as a number of different Cases (Case I, II, …, V). A summary of the WEC simulation results and environmental wave conditions used is given below:

1. Section 3.1 shows the response amplitude operators, force amplitude operators and relative capture width derived from simulations of regular waves (case I).

2. Sections 3.2 and 3.3 provide the minimum, maximum, and root mean squared (RMS) variation of flat-plate kinematics, PTO forces and power output for normal operational conditions. The wave conditions for these simulations have been represented by unidirectional irregular waves (case II) and spread irregular waves (case III).

3. Time series of peak loads during extreme simulations are provided in Section 3.4. The extreme sea states are defined in cases IV and V.

3.1 Regular waves

A series of simulations in regular waves were conducted in order to compute the response amplitude operators (RAO) for the flat-plate kinematics, the relative capture width of the point absorber and the force amplitude operator (FAO) on the PTO. The response or force amplitude operator is defined by X/a where a is the wave amplitude. A range of regular wave periods and amplitudes were used to conduct simulations.

The response and force amplitude operators are calculated using the following equation for the amplitude of response or force:

$$X = \sqrt{2} \cdot SD[\hat{\phi}_i - \langle \hat{\phi}_i \rangle] \tag{3}$$

where $\hat{\phi}_i$ is a time history of the point absorber motions and forces for $i = x, y, z, Rx, Ry, d$ and all frequencies except the fundamental frequency have been removed from the signal. The operators SD and $\langle \rangle$ are the standard deviation and mean of the time series output. The signal processing, includes curtailing the simulation ramp-up time and calculating the moving mean of the signal, where the window is equal to the regular wave period. The time series is curtailed to a duration of 25 times the wave period. This curtailed time series is taken from the end of the time series to ensure that transients in motions and forces are not included.

For each wave amplitude and period the ratio of wave height H to wavelength λ (or wave steepness, see /8/) was computed.

$$\epsilon = H/\lambda \tag{4}$$

An upper limit to the wave steepness $\epsilon = 1/7$ was imposed similar to the analysis in /7/. All results under the wave breaking limit are included in the analysis.

As the wave conditions considered in this section are unidirectional, the results for flat-plate sway and roll motions have not been included. This type of motion is not expected for these wave conditions and analysis of the time series data found that the flat-plate roll and sway motions were negligible.

The heave RAO of the flat-plate is calculated using the ϕ_z kinematics and is illustrated in Figure 3-1. It can be seen from the invariant RAOs that the global flat-plate heave is linear with respect to wave amplitude (as expected from the linearity of the hydrodynamics and structural constraints in this degree of freedom). The resonance in the heave motion of the flat-plate was designed to occur close to an angular frequency of 0.9 rad/s, which corresponds to a 7 s wave period. However, no peak can be seen in the RAO and it is assumed that this is because of the large radiation damping (b_{33} =577 Ns/m for $\omega = 0.9$ rad/s). Another possible explanation for the lack of a resonant peak could be due to coupled motion. Coupled motion may cause a deviation in the resonant frequency ω which was derived assuming uncoupled heave motion. However, in this case, it is not thought that this explains the lack of resonance peak as the RAO of heave motions appears linear. At low angular frequencies or long wave periods (>7 s), the flat-plate tends to follow the incident wave elevation and the RAO tends to unity. In contrast, for short period waves (<5s) the flat-plate does not respond significantly to incident wave excitation. These features of the response are expected for wave energy devices and in particular point absorbers.

The global surge and pitch RAOs are derived from the ϕ_x and ϕ_β motions of the flat-plate and are presented in Figure 3-2 and Figure 3-3, respectively. The surge response is strong and nonlinear in long period waves. The global flat-plate pitch response is linear and the large water plane area of the flat-plate results in small pitch motions. The surge RAO for surge also indicates a long period resonance which is associated with rotation around the anchor point.

From observations of the time series data, the long period wave scenarios reveal instances of a period doubling in the global surge motions as shown in Figure 3-4. This reveals that, when excited by long period waves, the device spends one wave period downwave of the anchor point and another upwave of the anchor point and so on. For shorter wave periods, period doubling of the flat-plate motions does not occur but instead the device moves to a downwave position and oscillates around this point.

The force amplitude operator (FAO) has been computed using the PTO applied force. The results are shown in Figure 3-5 and reveal that the greatest loading occurs due to incident waves with a period of approximately 10.5 s. At lower frequencies the FAO shows nonlinear motions most likely related to the nonlinear surge motions.
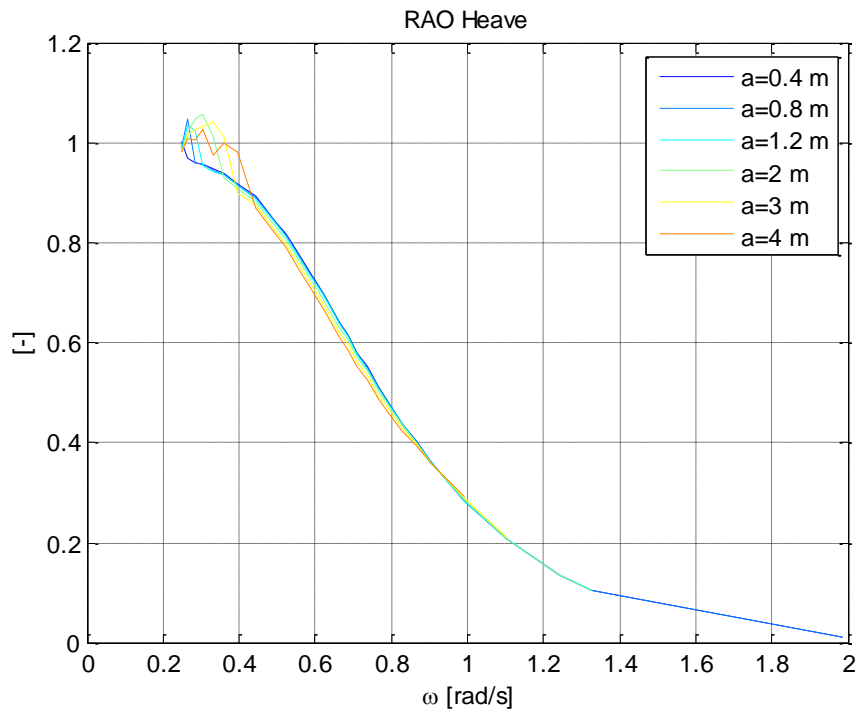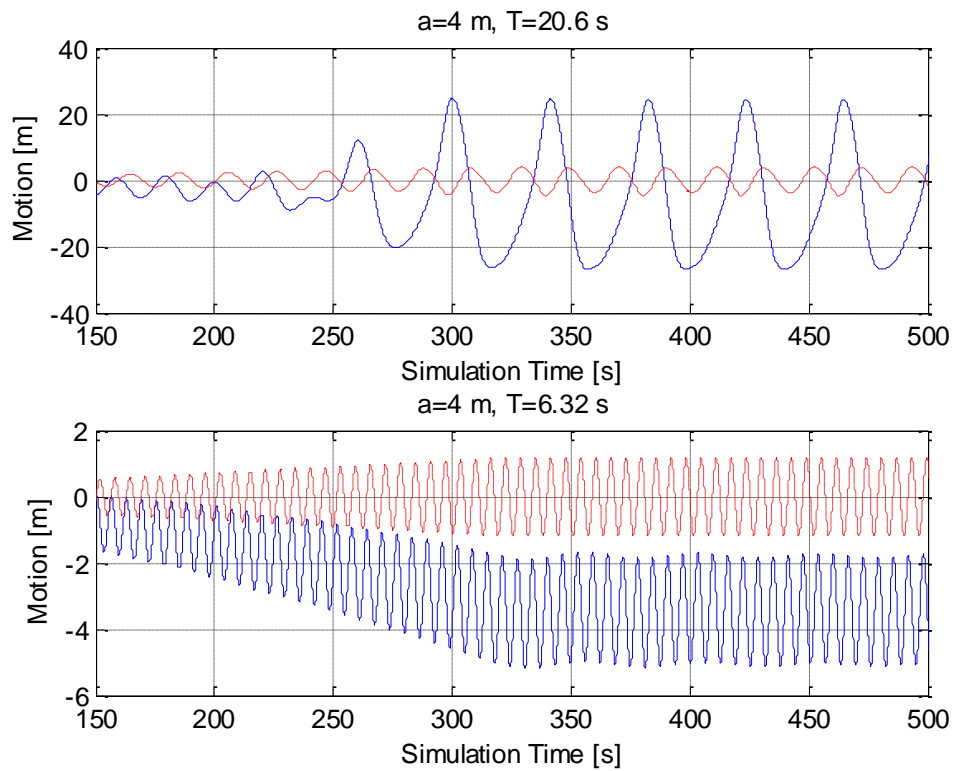
Figure 3-1 Response amplitude operator of flat-plate global heave.
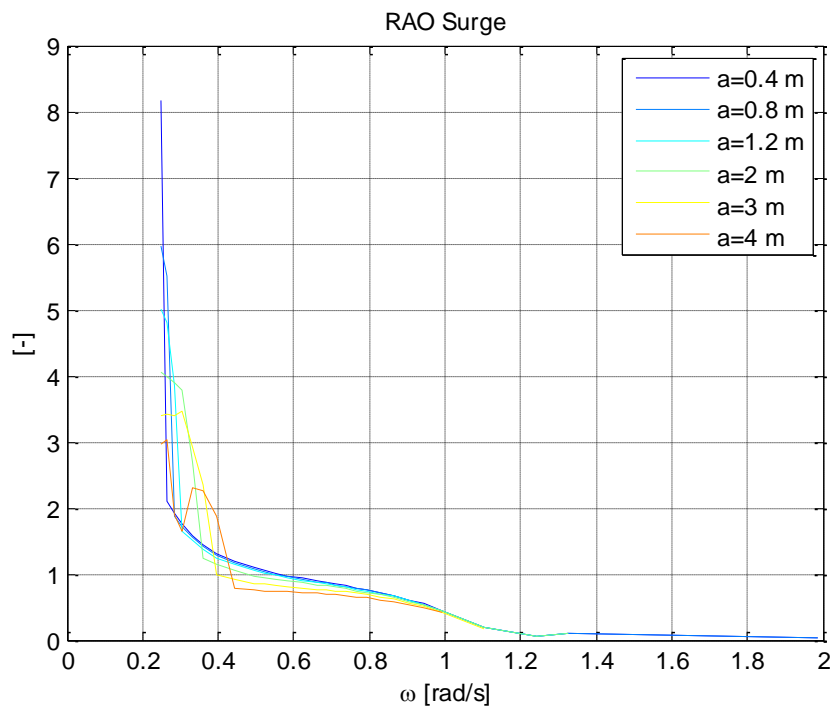
Figure 3-2 Response amplitude operator of flat-plate global surge.
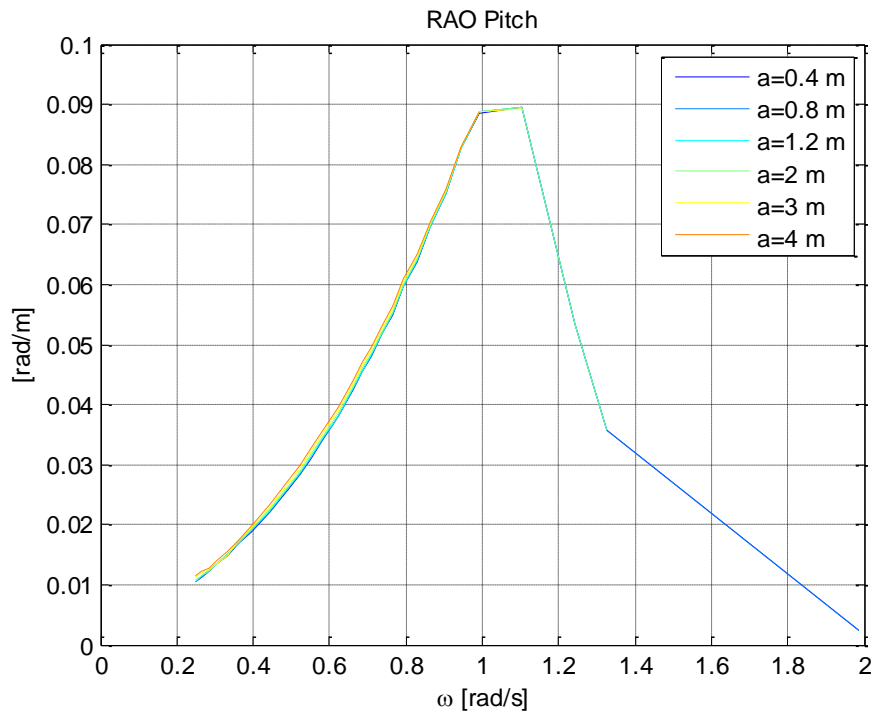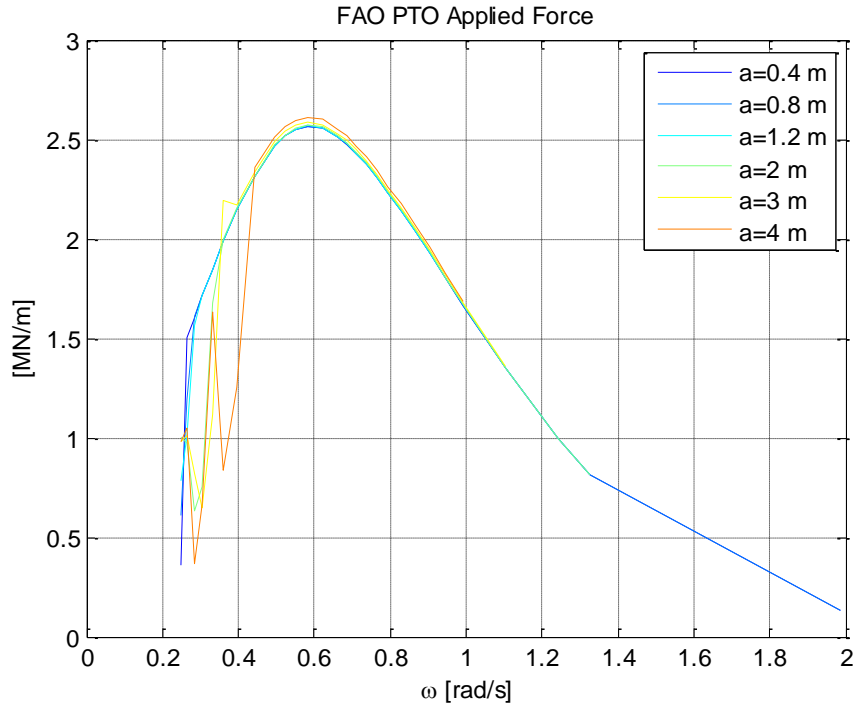
Figure 3-3 Response amplitude operator of flat-plate global pitch.

Figure 3-4 Time series plot of flat plate motions for simulations with long period regular waves (top diagram T=20.6 s) and low period regular waves (bottom diagram T=6.32 s). The blue line is flat-plate global surge and red dashed is global heave.

Figure 3-5 Force amplitude operator of PTO.

The capture width (l) is calculated using the 'Total System Power Take-Off (PTO) Performance' (PTO Power Output P) and dividing by the incident wave power per unit width P_w such that

$$l = \frac{P}{P_w} \tag{5}$$

Assuming deep water, the incident wave power is given by:

$$P_w = \frac{\rho \pi g^2 H^2 T}{8} \tag{6}$$

The relative capture width of the flat-plate is therefore given by $r = l/D$, where D is the diameter of the flat-plate. The relative capture width is shown in Figure 3-6. The largest power output is observed at 0.7 rad/s (wave period of 6 s) with the device extracting up to 1.5 times of the incident wave power passing through its width (albeit for a very narrow band of frequencies).
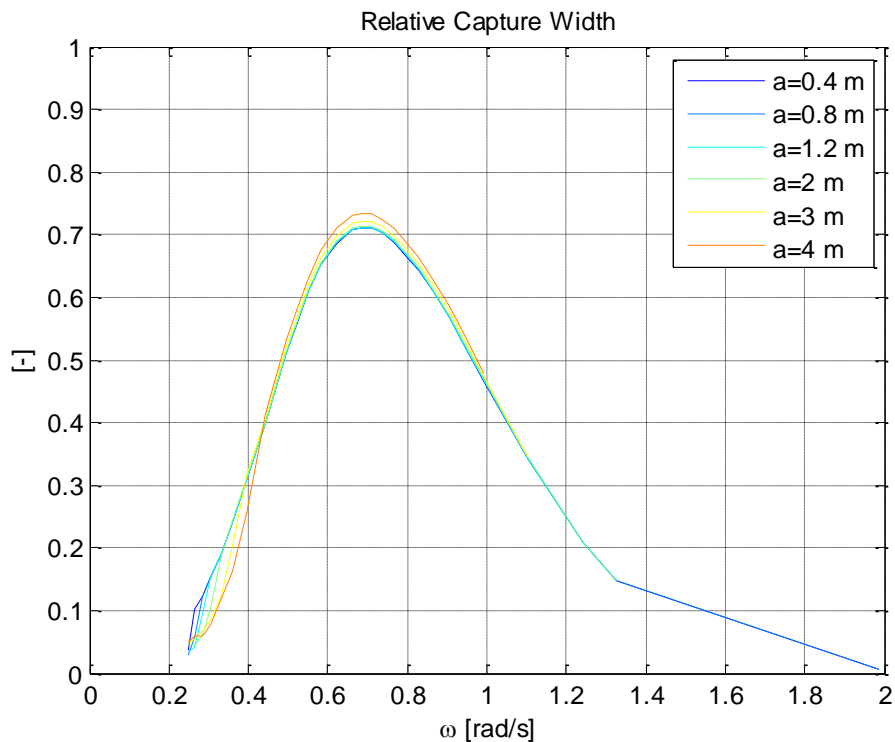
Figure 3-6 Relative capture width of point absorber.

3.2 Unidirectional irregular sea states

Time domain simulations were conducted with irregular unidirectional waves (Case II). The minimum and maximum values throughout the time series are presented for the flat-plate kinematics, PTO forces and power output. The simulations have been run for 3 hours (equivalent full scale duration) in order to obtain reliable estimates of extreme values.

The maximum global motions of flat-plate heave, pitch and surge are summarised in Figure 3-7, Figure 3-8 and Figure 3-9 respectively. Assuming deep water waves, the significant wave steepness S_e is given by

$$S_e = \frac{2\pi H_s}{gT_e^2} \tag{7}$$

where H_s is the significant wave height, T_e the energy period and g is the acceleration due to gravity. This formula is simply the wave steepness equation but written in terms of mean wave parameters H_s and T_e. An upper limit for S_e is derived using the limit for individual wave steepness $\epsilon < 1/7$. A link is formed between the maximum individual wave height and the significant wave height such that $0.5H_{max} = H_s$. Using Equation (4) to rewrite ϵ in terms of H_s a suitable limit for S_e is given by $S_e < 0.5 \times 1/7 = 0.07$. The significant steepness is calculated for all sea states and then the limit is applied to curtail information derived for sea states that are unrealistic.

It can be seen that as the incident significant wave height increases, the flat-plate motions also increase. The maximum global heave and surge excursions are greatest for long period waves. The flat-plate pitch motion is generally greatest for energy periods around 7 s which is in agreement with the shape of the RAO for pitch in Section 3.1.

The maximum values of the PTO joint extension and applied force acting on the PTO joint are shown in Figure 3-10 and Figure 3-11, respectively. The applied force on the PTO is greatest when the wave height is large and the energy period is around 10 s. The PTO applied force in the numerical model is negative when the PTO spring is in tension. As can be seen from Figure 3-11, for moderate significant wave height (H_s>1 m) there are instances when the tether is no-longer in tension. The maximum power output in Figure 3-12 shows a similar trend to the PTO applied force, with the largest power output close to an energy period of 11 s.

Minimum values of flat-plate motion for heave, pitch and surge are summarised in Figure 3-13, Figure 3-14 and Figure 3-15, respectively. The largest negative values of flat-plate heave excursion are directly related to significant wave height and the minimum pitching motions are observed around 8 s. The minimum PTO displacement, PTO applied force and power absorption are presented in Figure 3-16, Figure 3-17 and Figure 3-18, respectively. The results show that the extreme displacements and forces acting on the device are approximately symmetric around the equilibrium position. The minimum power output of the device is 0 W across all sea states as there are times when the PTO velocity is 0 m/s and therefore power is not generated.

The root mean square (RMS) motions of the flat-plate are presented in Figure 3-19 and Figure 3-20, respectively.
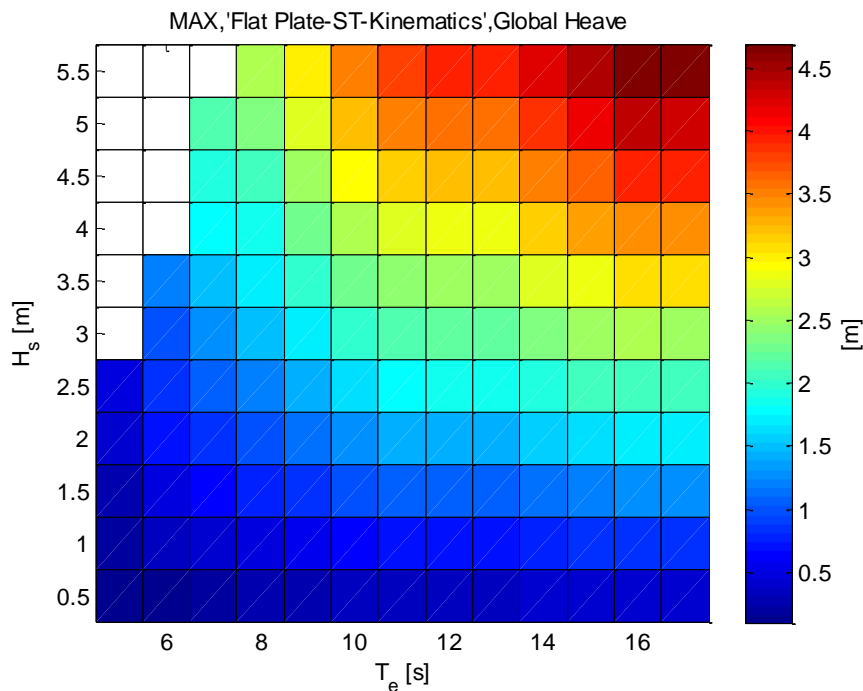
Figure 3-7 Max of global flat-plate heave for irregular unidirectional waves.
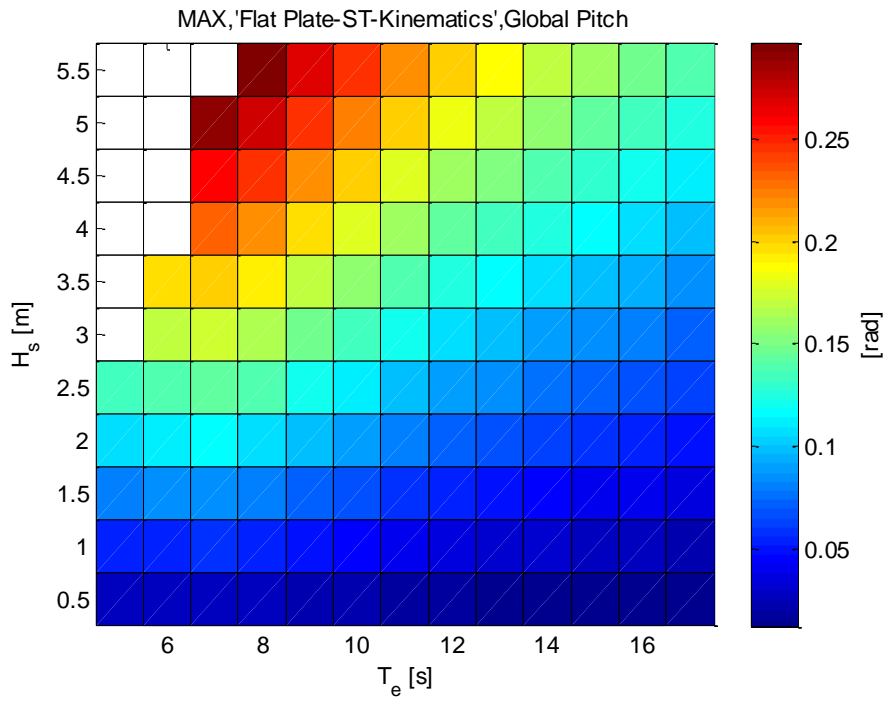
Figure 3-8 Max of global flat-plate pitch for irregular unidirectional waves.
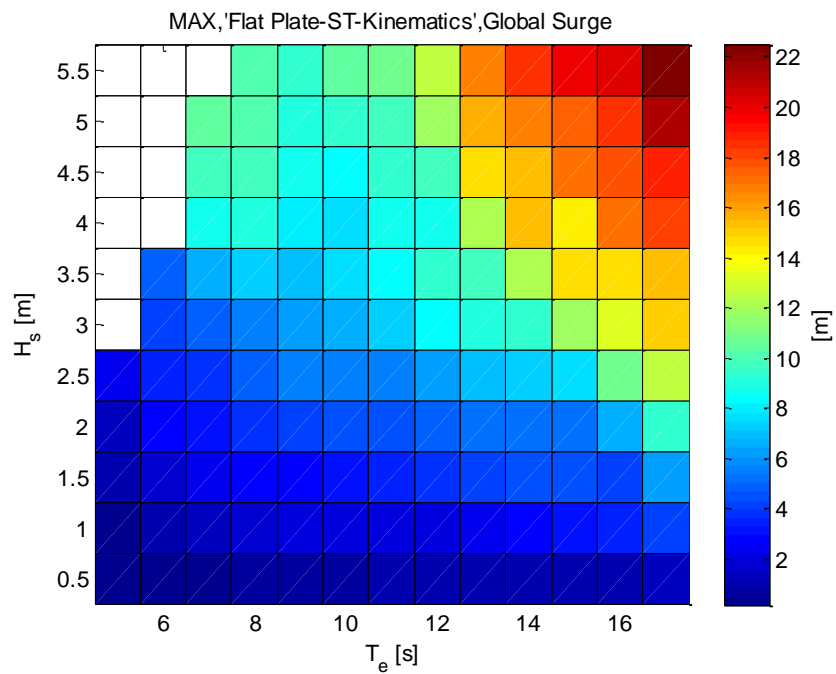
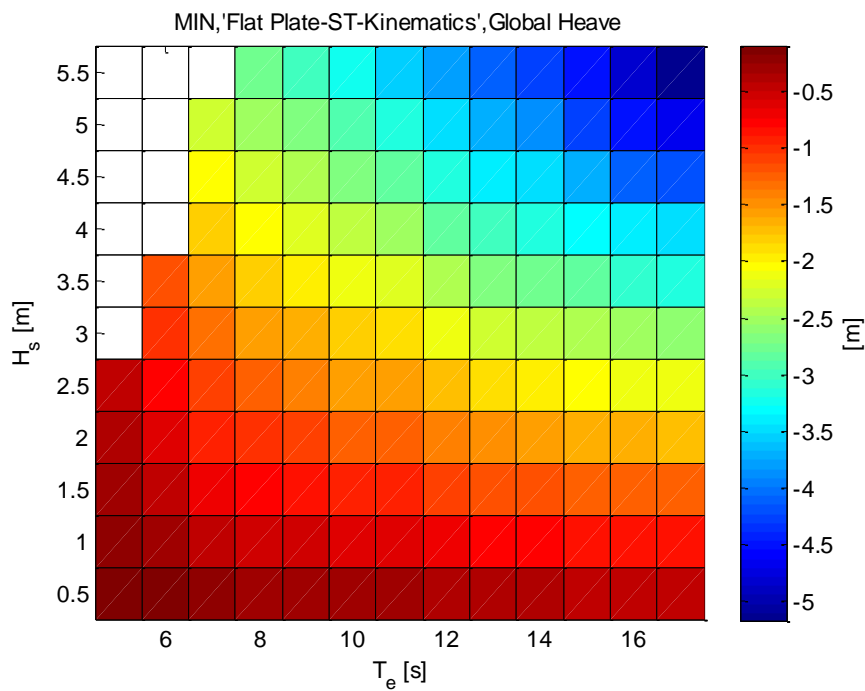**Figure 3-9 Max of global flat-plate surge for irregular unidirectional waves.**
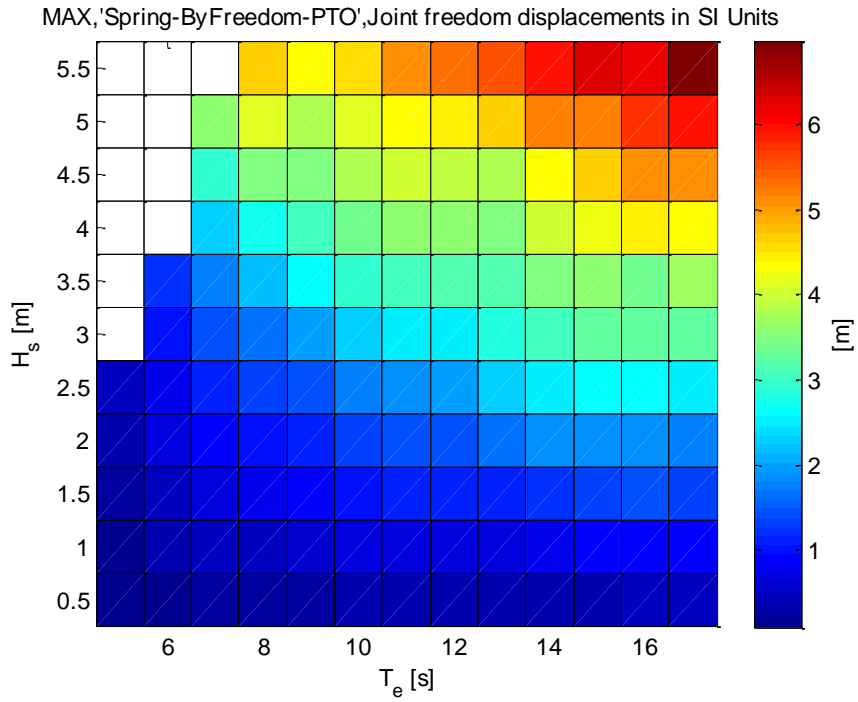
Figure 3-10 Max of PTO joint freedom for irregular unidirectional waves.
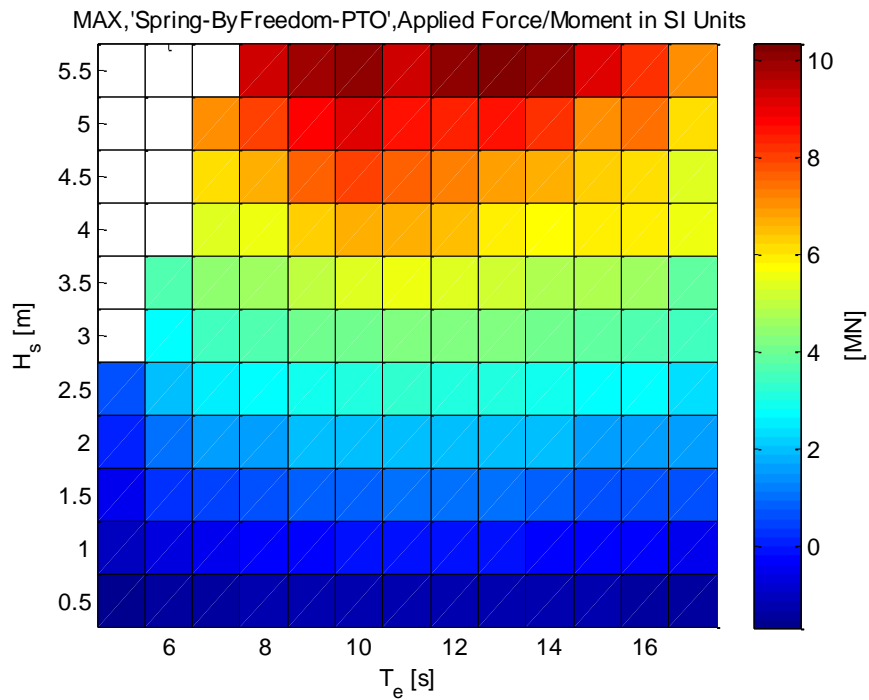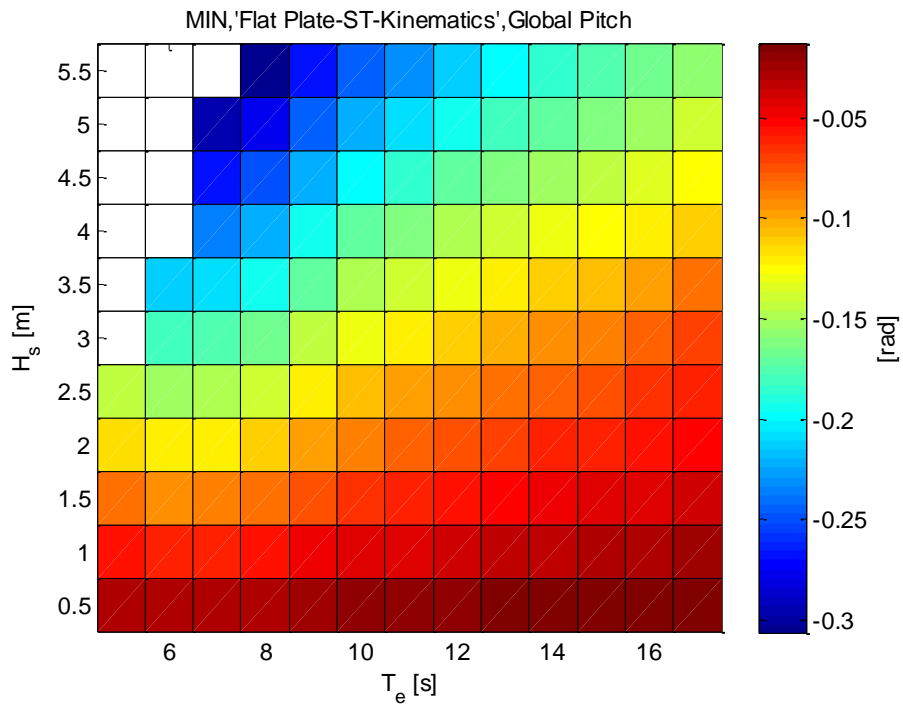

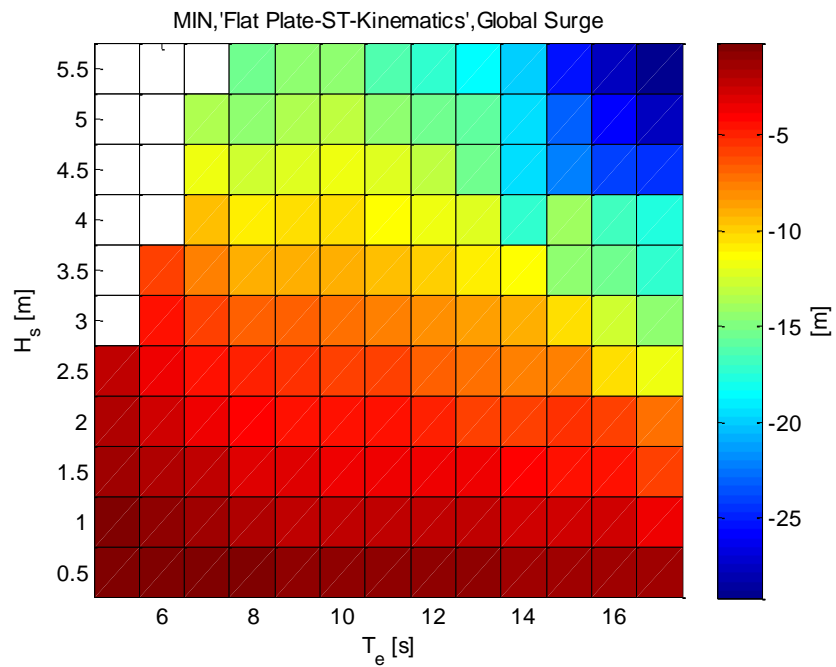**Figure 3-11 Max of PTO applied force for irregular unidirectional waves.**
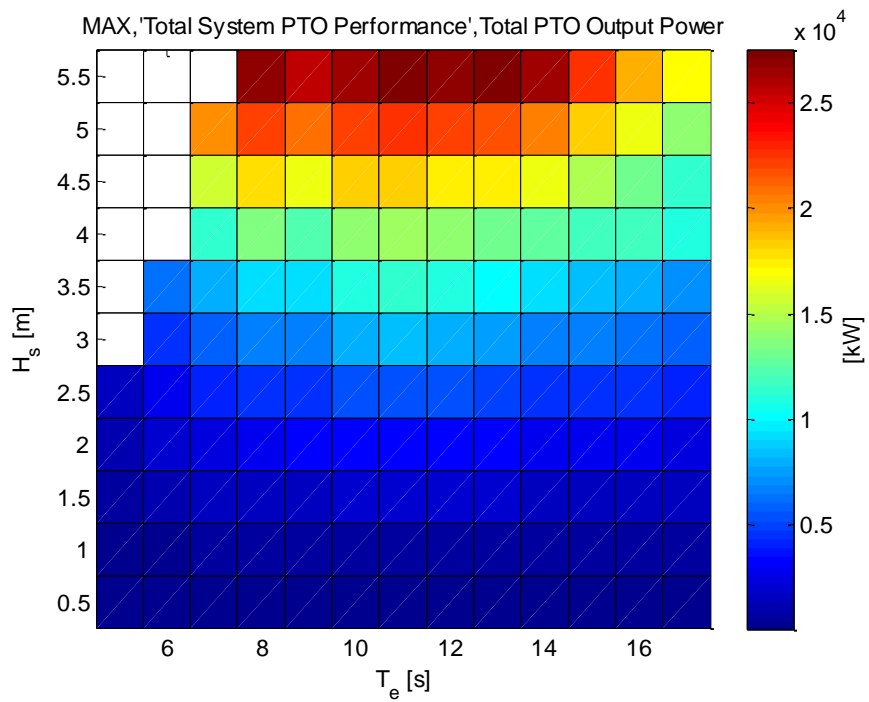
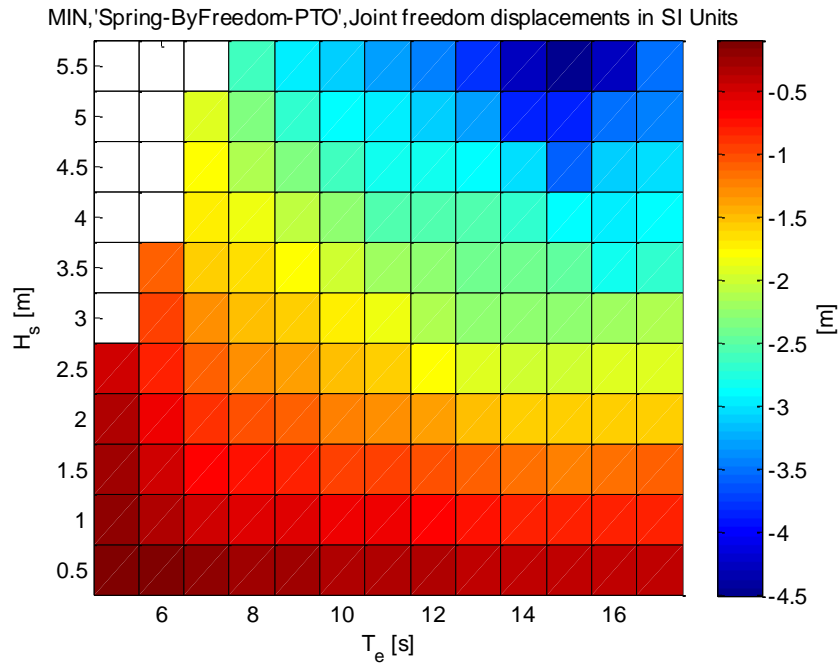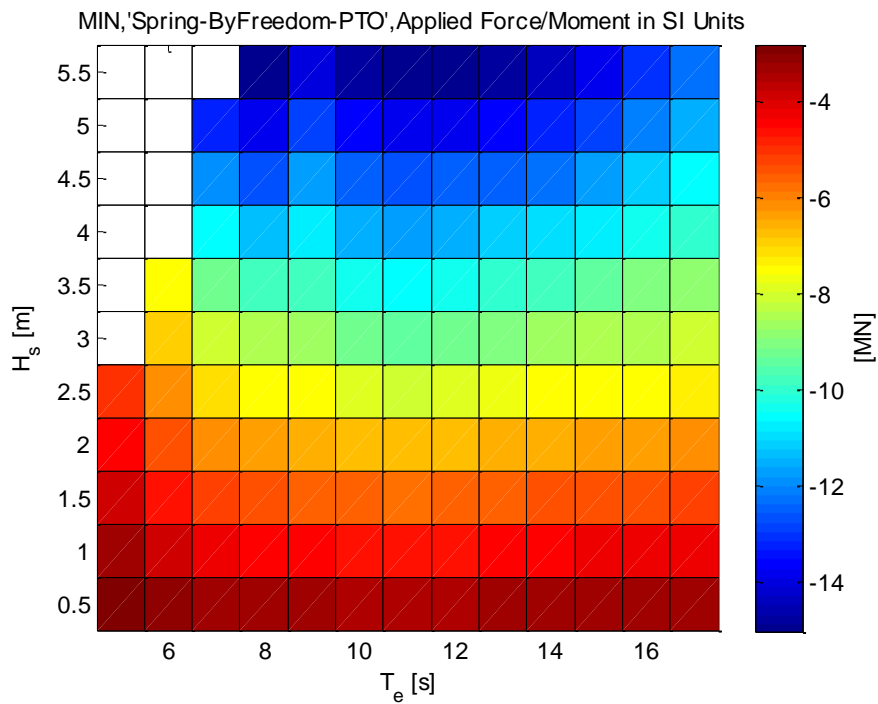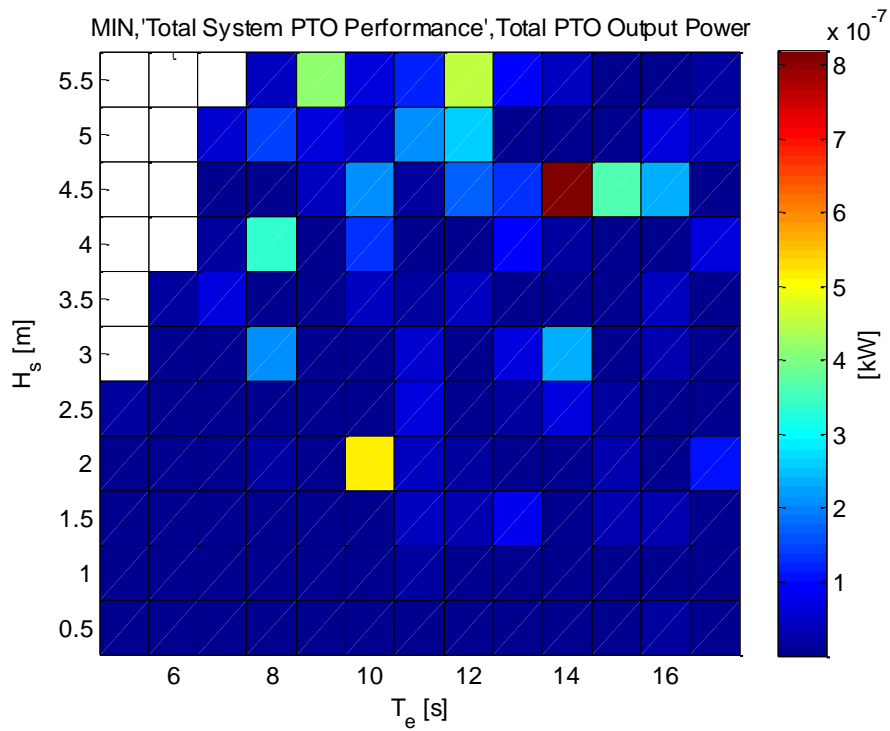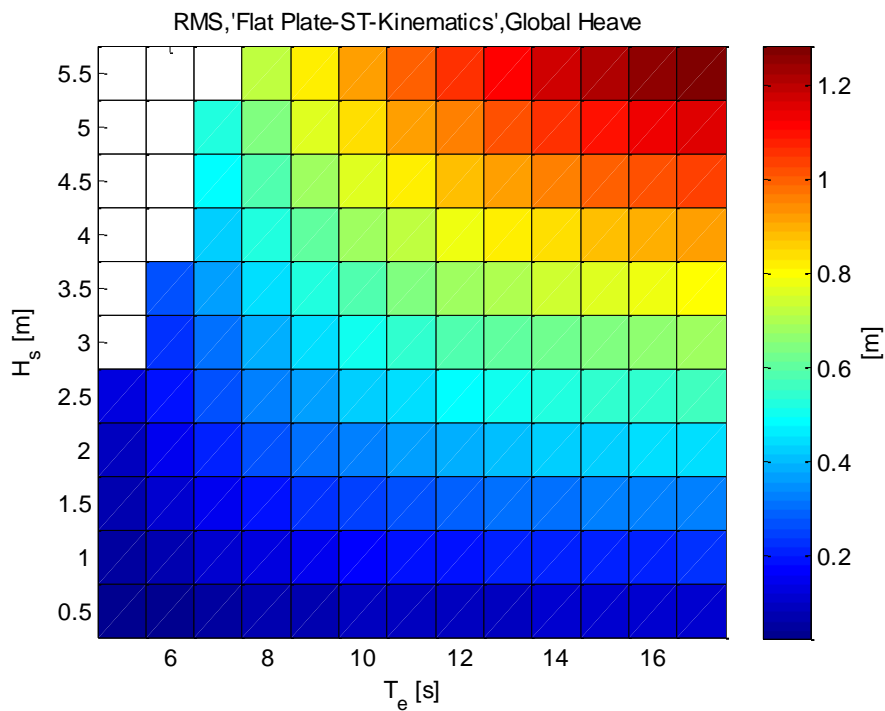**Figure 3-12 Max of PTO power output for irregular unidirectional waves.**

Figure 3-13 Min of global flat-plate heave for irregular unidirectional waves.

Figure 3-14 Min of global flat-plate pitch for irregular unidirectional waves.

Figure 3-15 Min of global flat-plate surge for irregular unidirectional waves.

Figure 3-16 Min of PTO joint freedom for irregular unidirectional waves.

Figure 3-17 Min of PTO applied force for irregular unidirectional waves.

Figure 3-18 Min of PTO power output for irregular unidirectional waves.

Figure 3-19 RMS of flat-plate heave for irregular unidirectional waves.
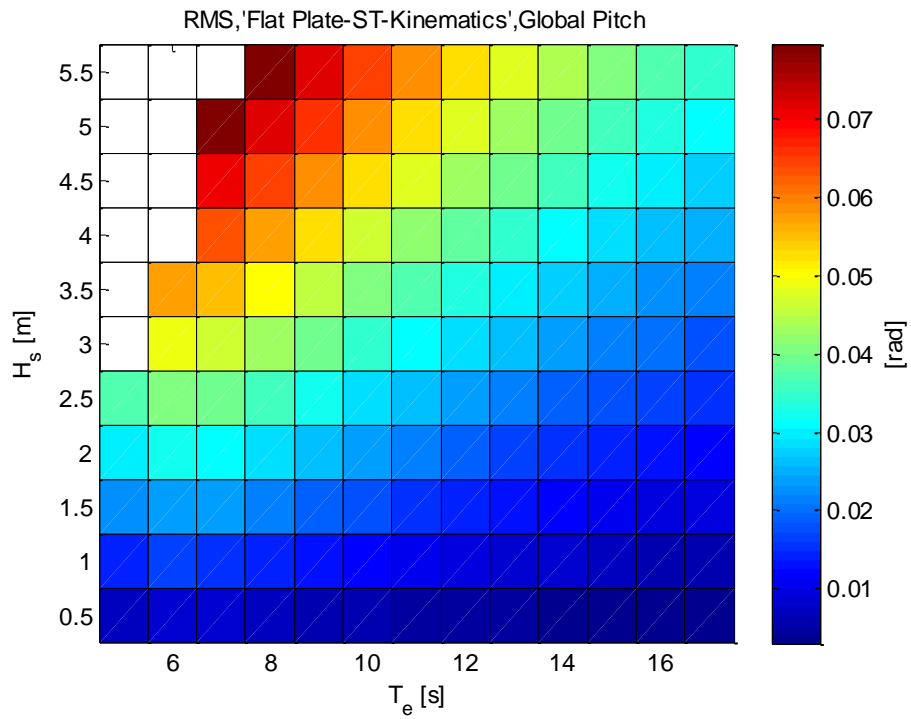
Figure 3-20 RMS of flat-plate pitch for irregular unidirectional waves.

3.3 Irregular spread waves

Time domain simulations were conducted with irregular spread waves (Case III). The simulations have been run for 30 minutes (full-scale equivalent duration). The RMS values of the time series results are presented for the flat-plate kinematics, PTO forces and power output. As before, the results must satisfy $S_e < 0.07$ such that all unrealistic sea states are removed.

The RMS of the flat-plate heave and pitch motions are presented in Figure 3-21 and Figure 3-22, respectively. The results of heave are similar to those in Section 3.2 with a similar range of motions observed. The RMS of pitch motions in the spread waves scenario is similar to the unidirectional case presented in Figure 3-20.

The multiple degree of freedom motion of the hinges (see Section 2) enable roll and global sway motions of the flat-plate to be captured. The RMS sway, surge and roll motions are presented in Figure 3-23, Figure 3-24 and Figure 3-25. The range of roll motion is small with the largest RMS values being around 2 degrees. The RMS surge and sway motions are also large with up to 7 m of motion for a sea state of H_s=5.5 m and T_e=16 s.

The time series of the flat-plate global sway and surge motions was analysed in detail for a sea state where the energy period and significant wave height was large (H_s=4 m and T_e=17 s). The power spectral density of the translational motions of the flat-plate are shown in Figure 3-26. In addition, the JONSWAP wave spectra has also been used for comparison. The plot reveals that the angular frequency of the sway and surge harmonics with the largest amplitude is much smaller than either the wave spectra or the heave motion of the device. In addition, the surge and sway motions are much larger than the heave motions. It is possible that in reality viscous effects which are not modelled in the simulations would damp this motion.

The RMS of the PTO joint displacement and applied force are provided in Figure 3-27 and Figure 3-28, respectively. It can be seen that the spring freedom and applied force is sensitive to both wave period and wave height.
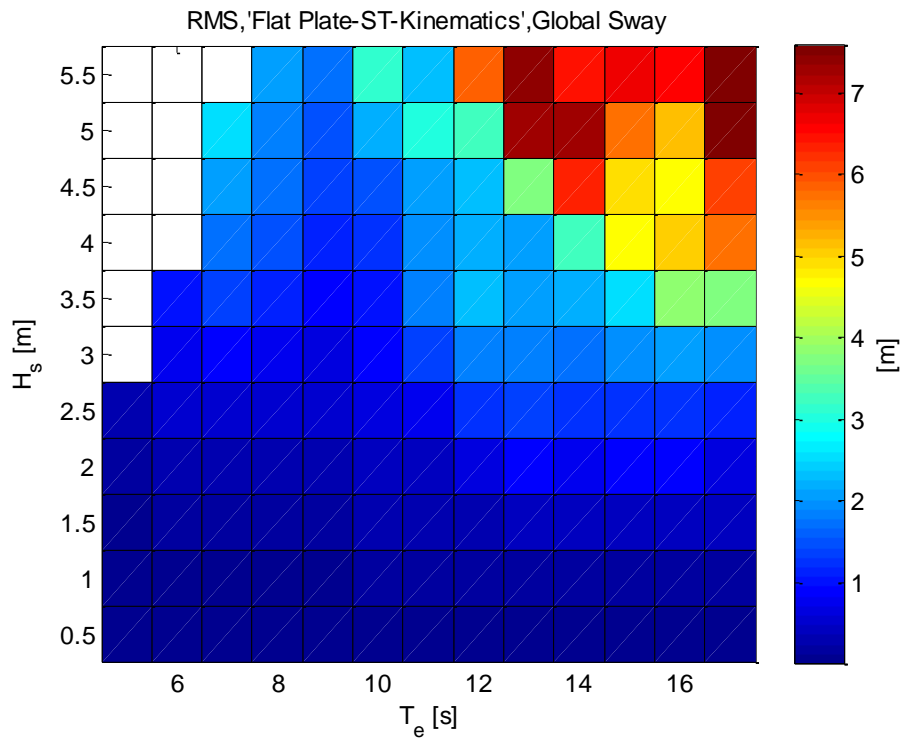
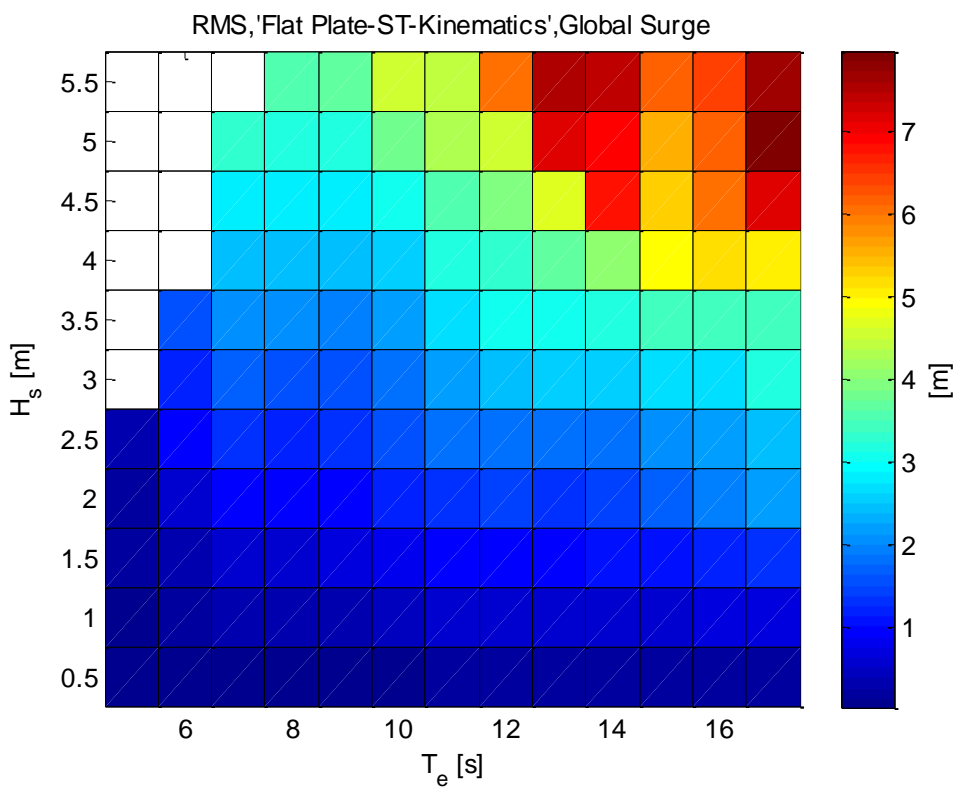The RMS and Mean of total PTO power output is presented in Figure 3-29 and Figure 3-30.
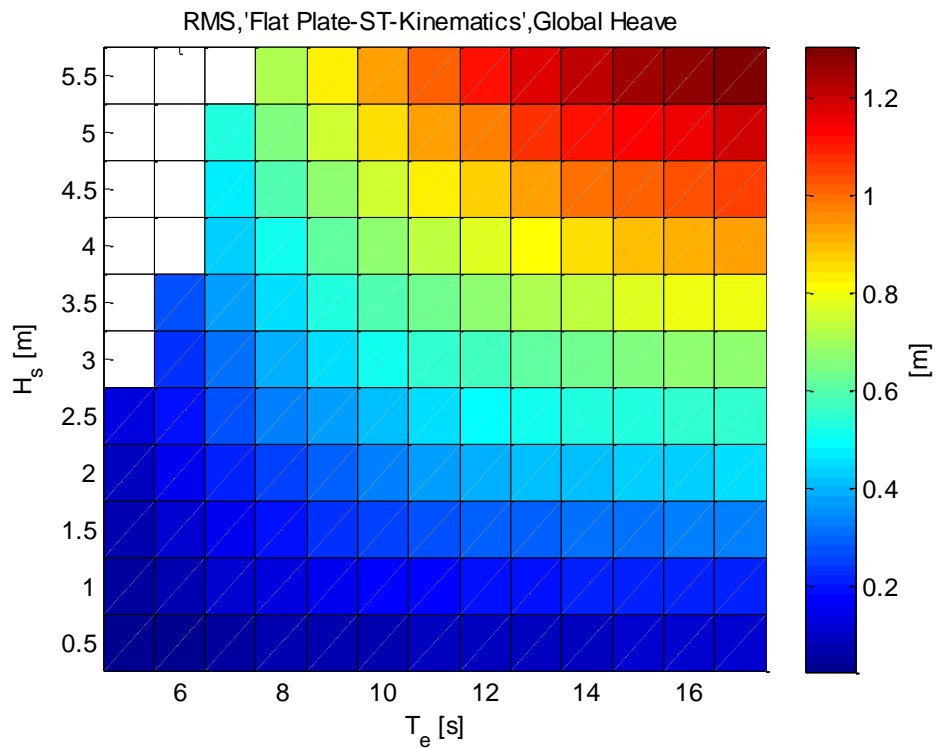
Figure 3-21 RMS of global flat-plate heave for irregular spread wave conditions.
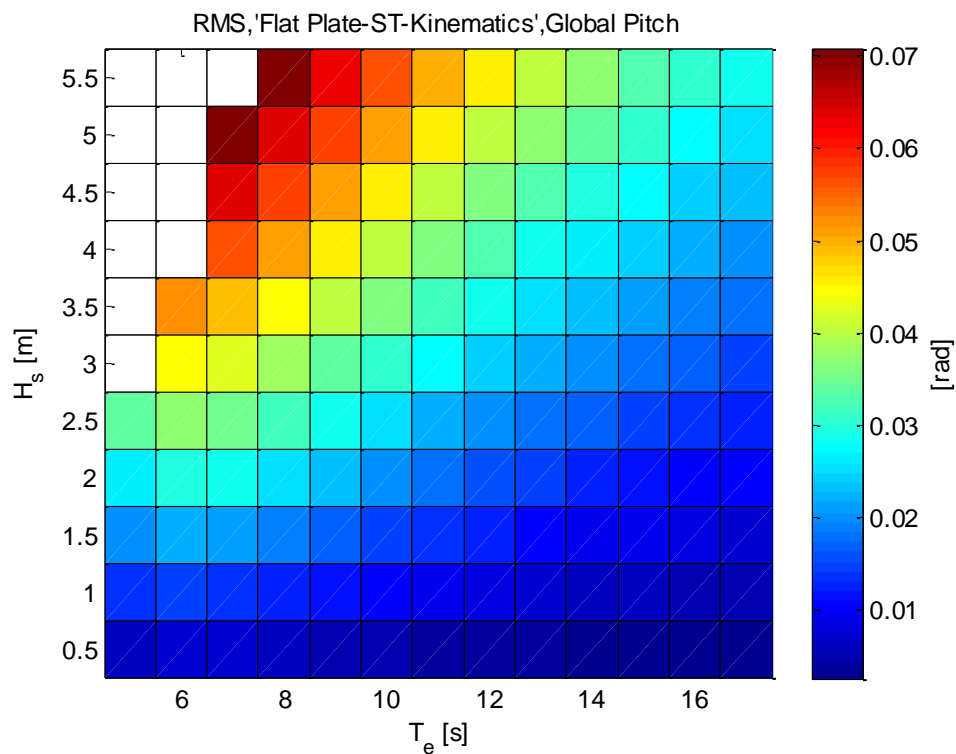
Figure 3-22 RMS of global flat-plate pitch for irregular spread wave conditions.

Figure 3-23 RMS of global flat-plate sway for irregular spread wave conditions.

Figure 3-24 RMS of global flat-plate surge for irregular spread wave conditions.
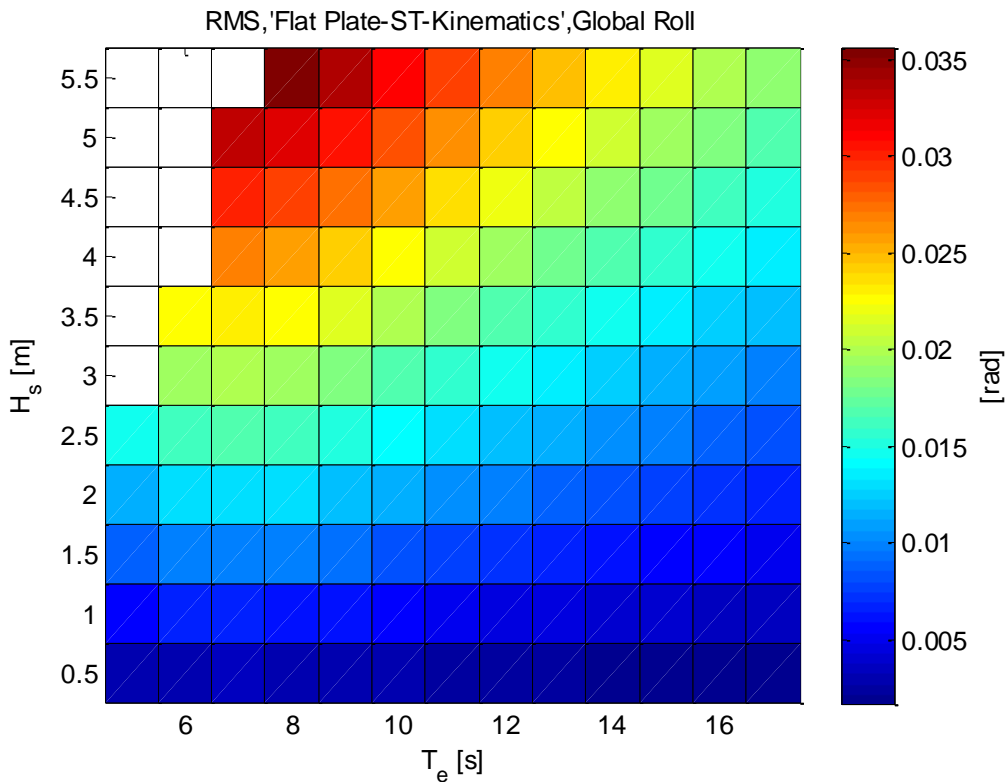
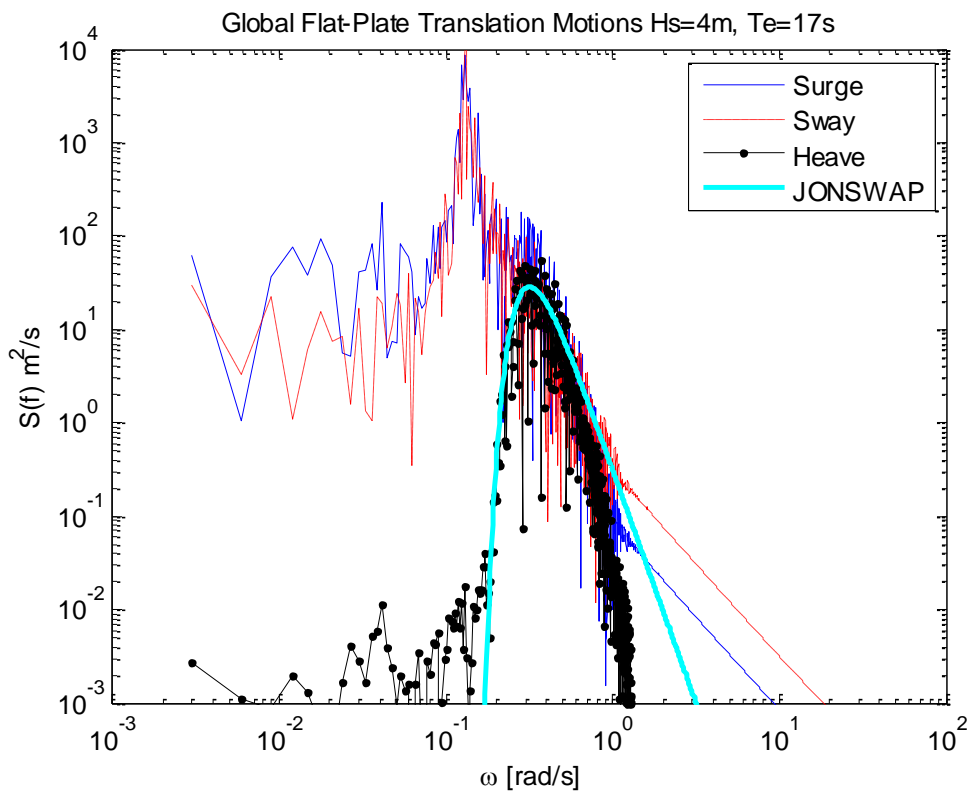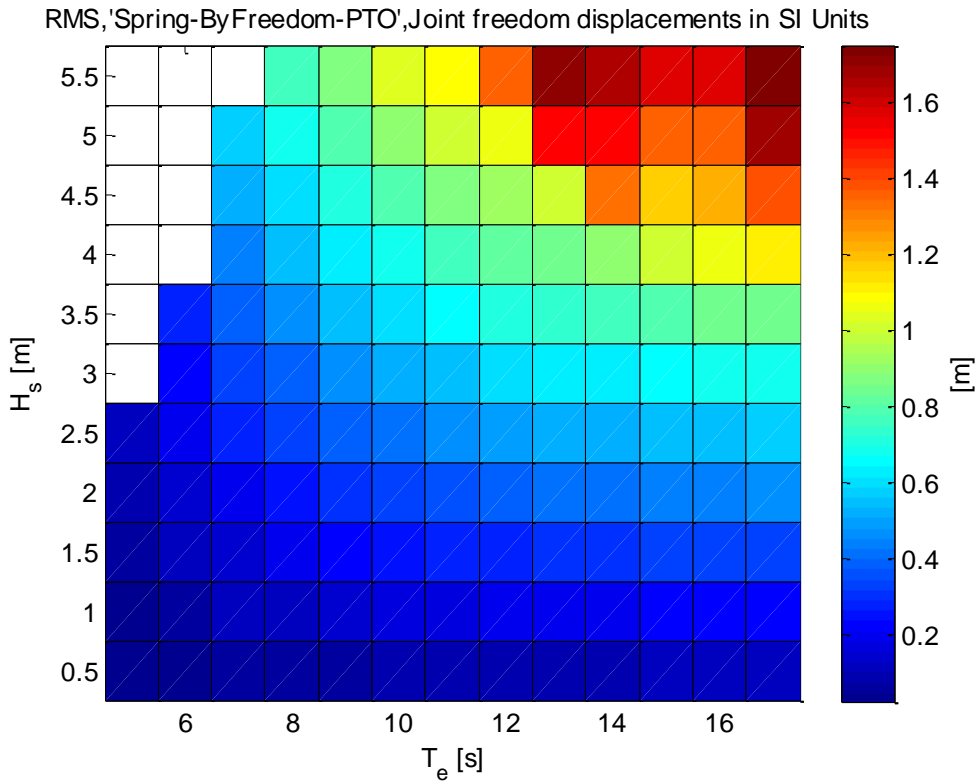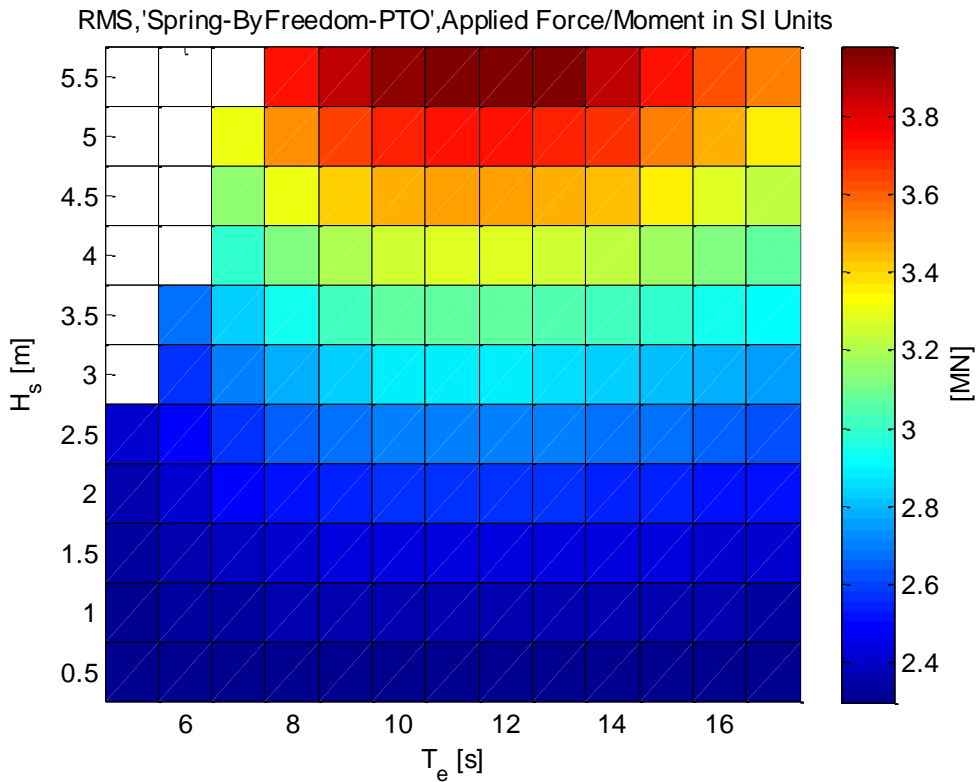**Figure 3-25 RMS of global flat-plate roll for irregular spread wave conditions.**

Figure 3-26 Power spectral density of global translational motions of flat-plate in the sea state H_s=4 m and T_e=17 s.

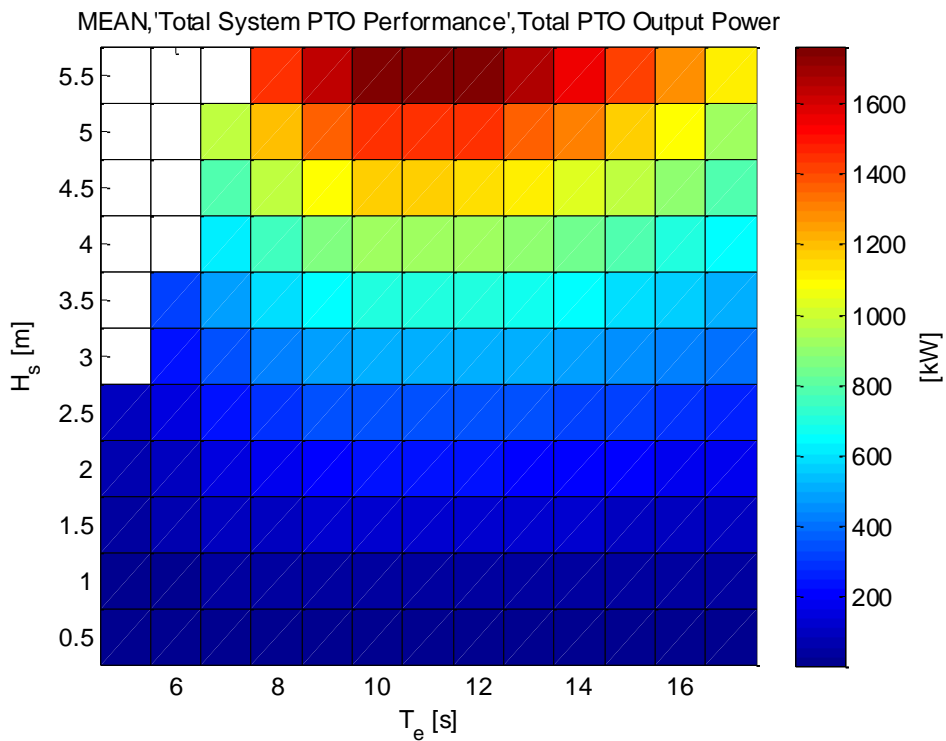RMS,'Spring-ByFreedom-PTO',Joint freedom displacements in SI Units

Figure 3-27 RMS of PTO joint displacement for irregular spread wave conditions.

RMS,'Spring-ByFreedom-PTO',Applied Force/Moment in SI Units

Figure 3-28 RMS of PTO applied force for irregular spread wave conditions.
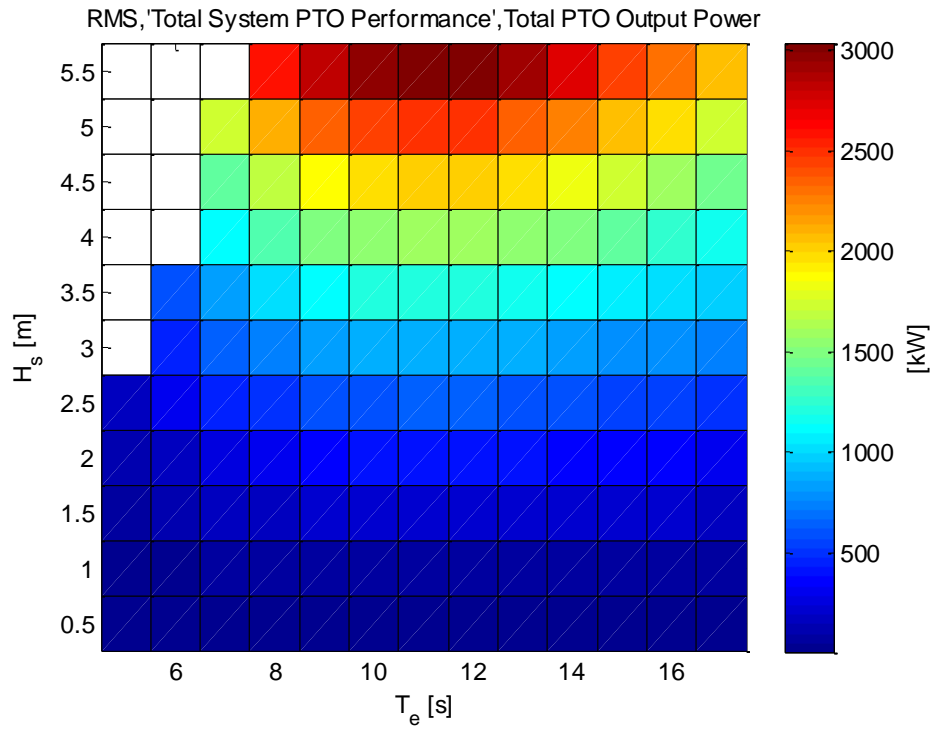
Figure 3-29 RMS of power output for irregular spread wave conditions.

Figure 3-30 MEAN PTO power output for irregular spread wave conditions.

3.4 Extreme response analysis

This section considers the device response to extreme wave conditions. Time domain simulations were conducted using the wave conditions described in Case IV.

The loading on a WEC depends on incident wave elevation and motion time history. An incident irregular wave field which describes normal operational conditions could yield a larger load than these extreme conditions. The time domain simulation where the largest force on the PTO unit occurs will be analysed. The maximum PTO load is a useful statistic for quantifying the maximum load the WEC must survive. This is often referred to as the ultimate limit state (ULS). The ULS is derived from analysis of simulations outputs during normal operational wave conditions in Section 3.4.1 and extreme conditions in Section 3.4.2.

3.4.1 Normal operational sea states

Time series data from numerical simulations conducted using the normal operational conditions described for case II were analysed to identify the sea state for which the maximum PTO load occurs. In the numerical model, the default PTO force is negative and therefore the maximum absolute value of the PTO force is used to identify the largest PTO loads. A 50 second sample was extracted around the point at which the maximum PTO load occurs. Figure 3-31 shows the time series output for the identified simulation. The maximum PTO load does not coincide with maximum heave. Instead it coincides with peak pitch, surge motion and (relative) maximum power extracted instead.
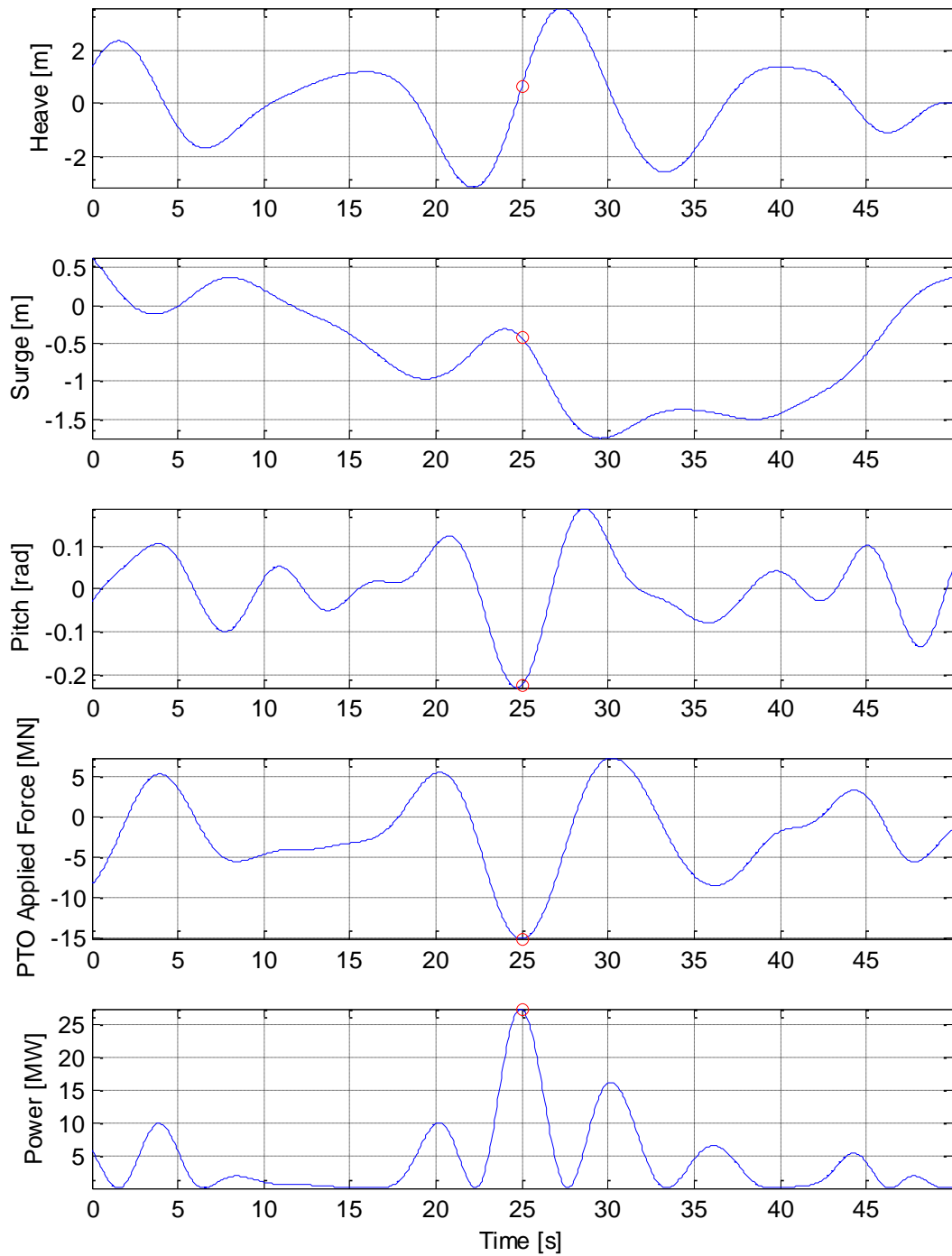
Figure 3-31 Time series of flat-plate position, load and power output around peak PTO applied force during normal wave conditions (case II) H_s=5.5 m and T_e=17 s.

3.4.2 Extreme sea states

A similar investigation was repeated for time domain simulations of extreme environmental conditions. This time, the sea state where the maximum PTO load occurred when simulating extreme sea states (case IV – see Appendix A) was identified. The time series data is presented in Figure 3-32. Again the peak load coincides with peak surge and pitch rather than heave.

Matrices of the extreme global flat-plate heave, pitch, PTO forces and power output are presented in Figure 3-33 to Figure 3-40.

A comparison of the minimum PTO loads that occur for each simulation of unidirectional normal waves and unidirectional extreme waves is shown in Figure 3-41. The extreme and normal conditions predict similar minimum loads however the spread of the results is much greater for the normal wave conditions.

The results are similar to those presented in Section 3.2. The flat-plate heave motion responds primarily to long period waves while the PTO loads and power output are sensitive primarily to the wave height.
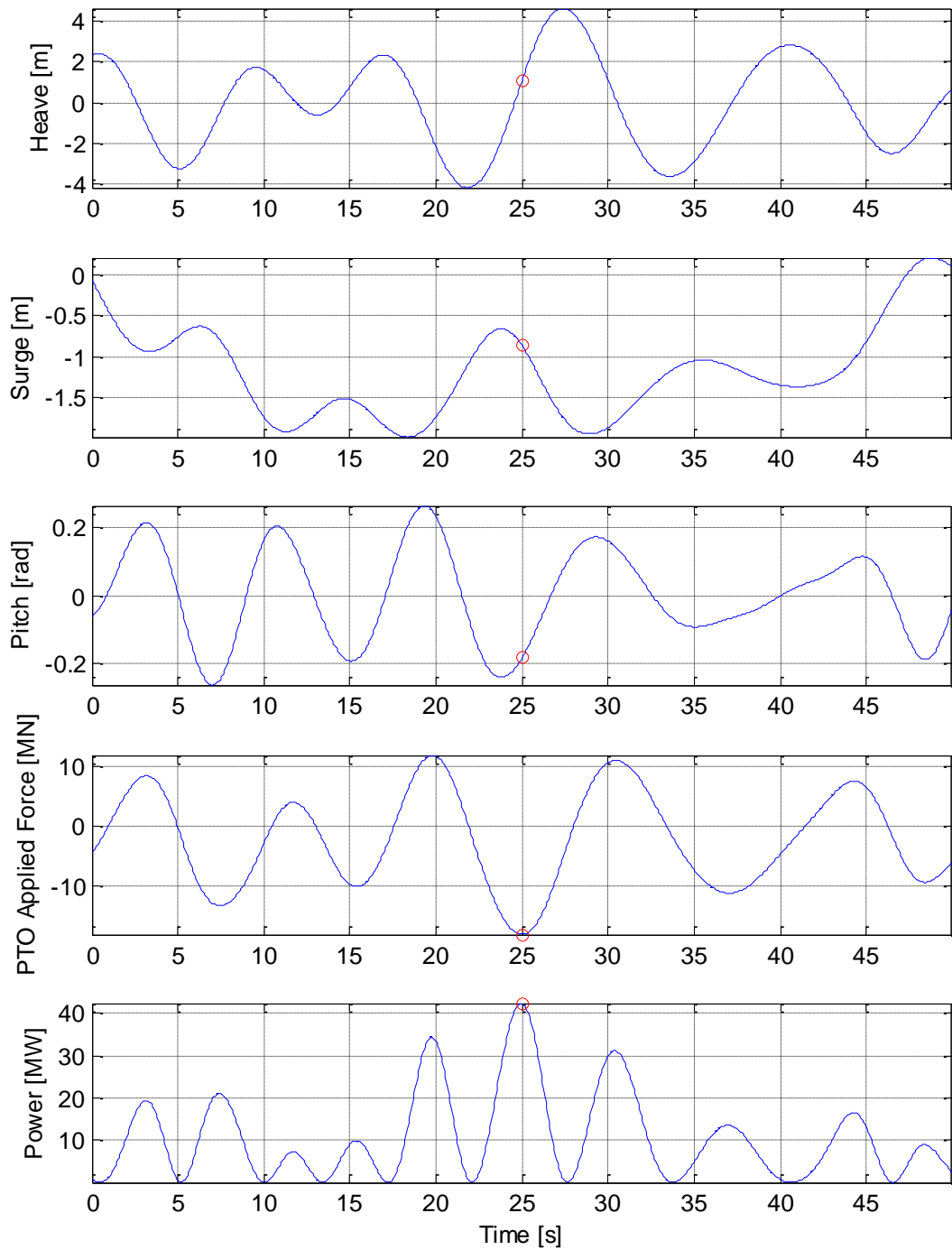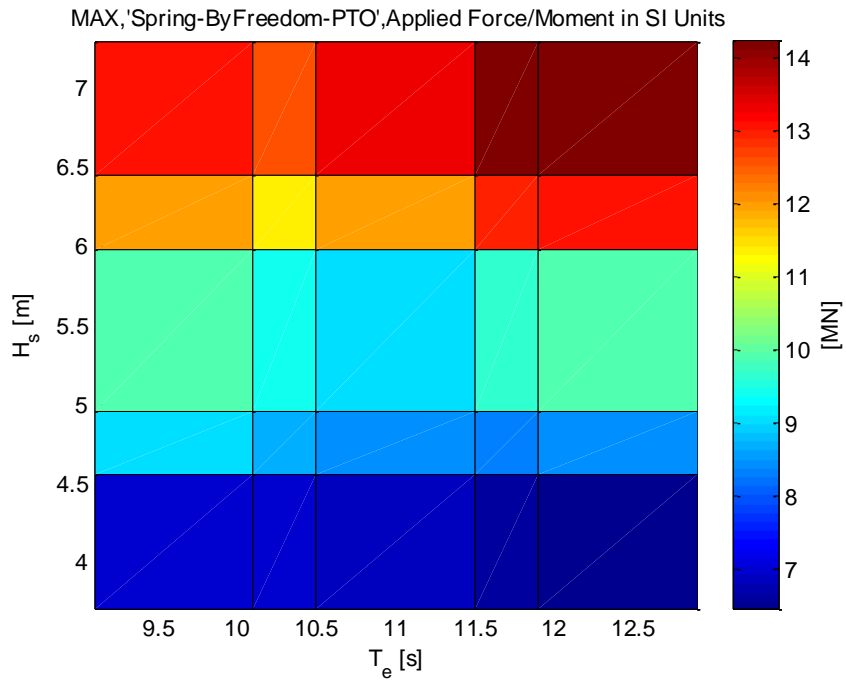
Figure 3-32 Time series of flat-plate position, load and power output around peak PTO applied force during extreme wave conditions (case IV) H_s=6.87 m and T_e=11.0 s.
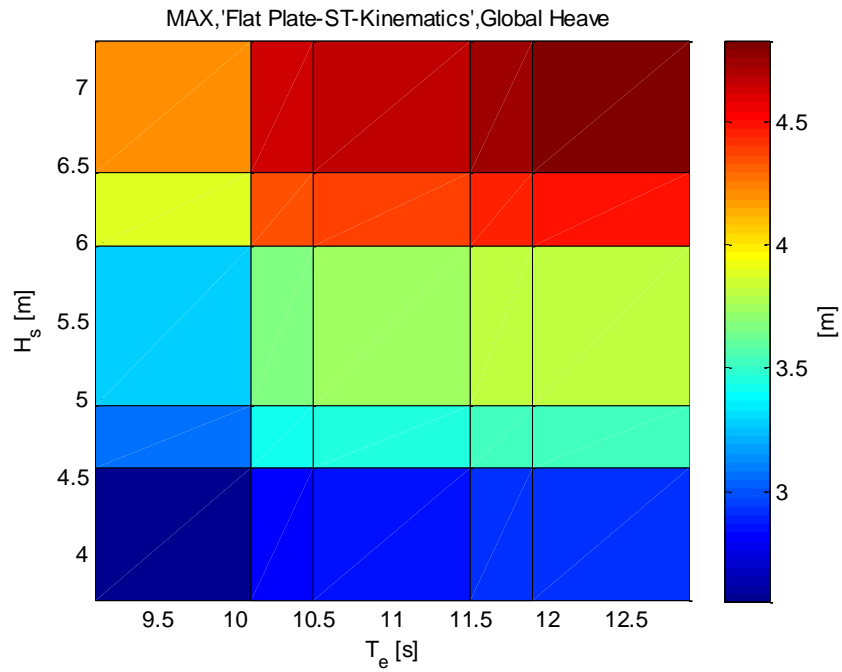
Figure 3-33 Max of global flat-plate heave for irregular unidirectional extreme waves
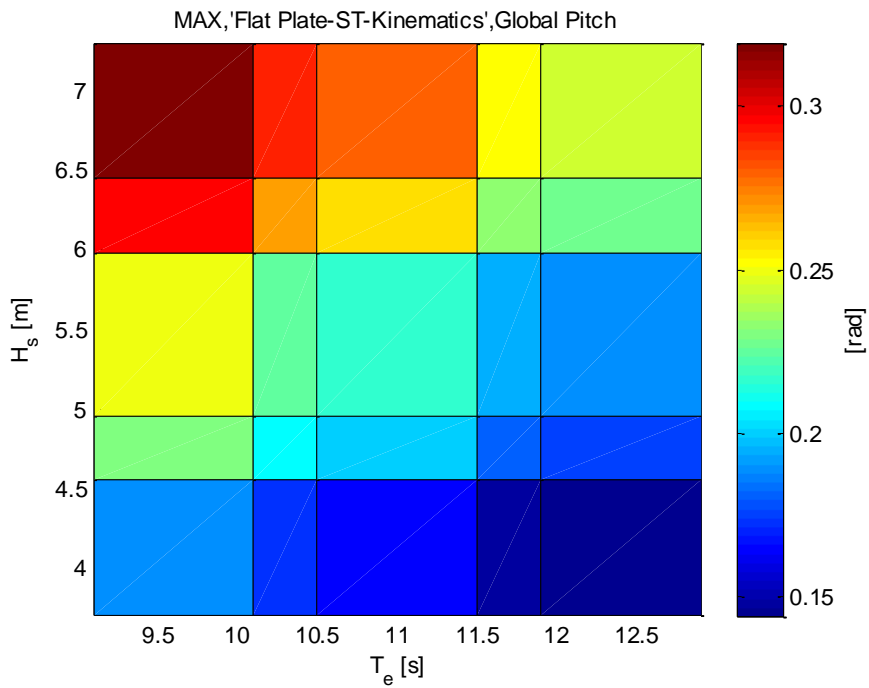
Figure 3-34 Max of global flat-plate pitch for irregular unidirectional extreme waves

Figure 3-35 Max of PTO applied force for irregular unidirectional extreme waves

Figure 3-36 Max of PTO power output for irregular unidirectional extreme waves
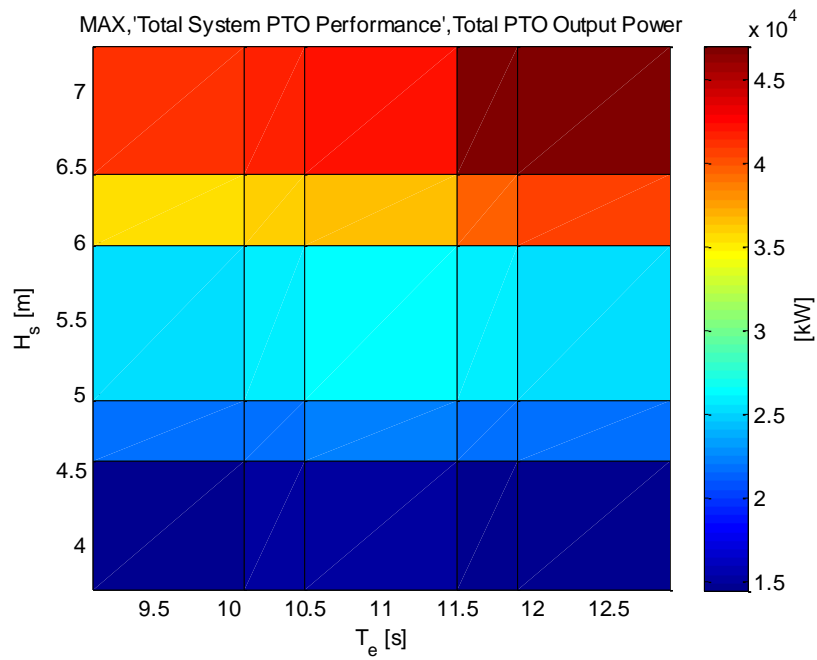
Figure 3-37 Min of global flat-plate heave for irregular unidirectional extreme waves
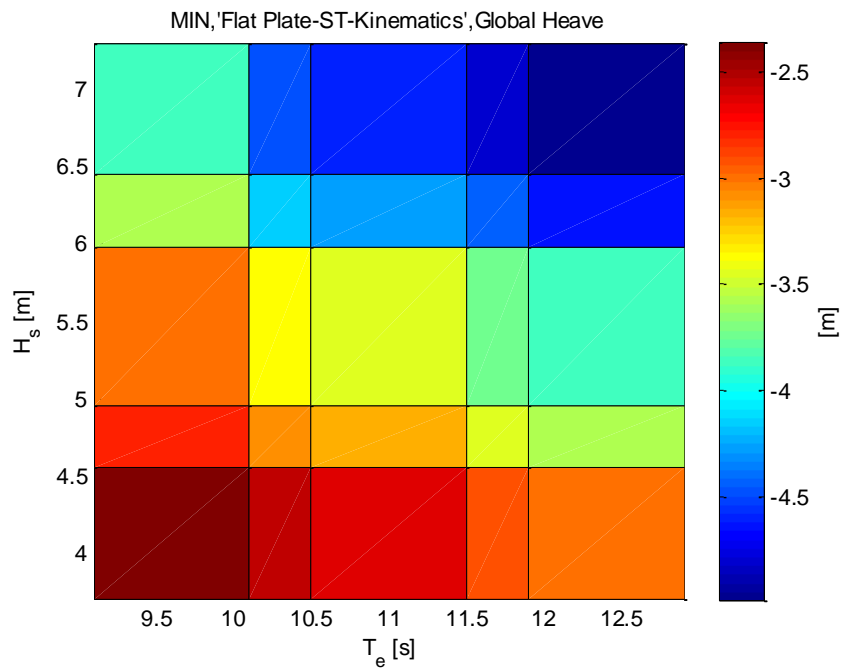

Figure 3-38 Min of global flat-plate pitch for irregular unidirectional extreme waves
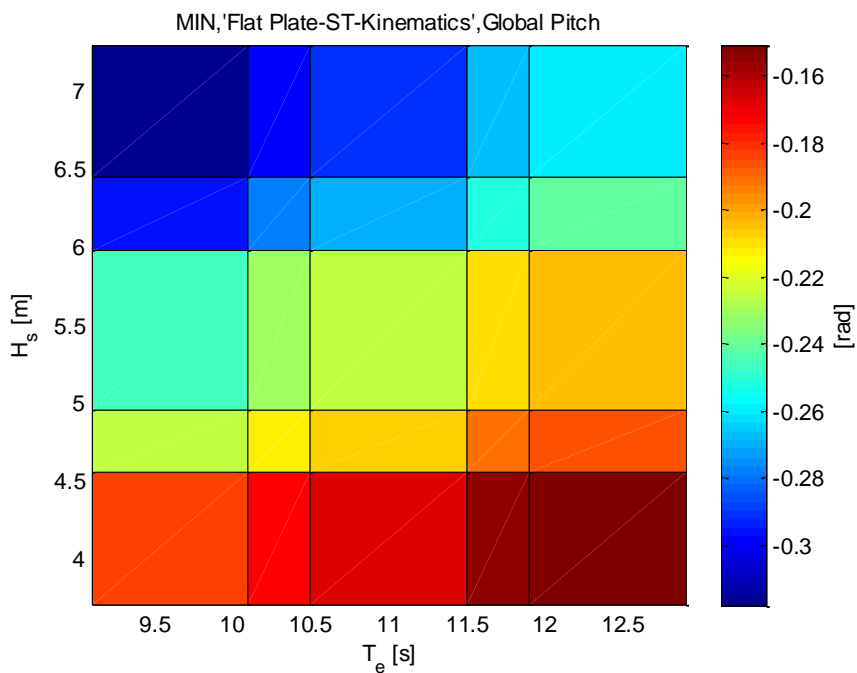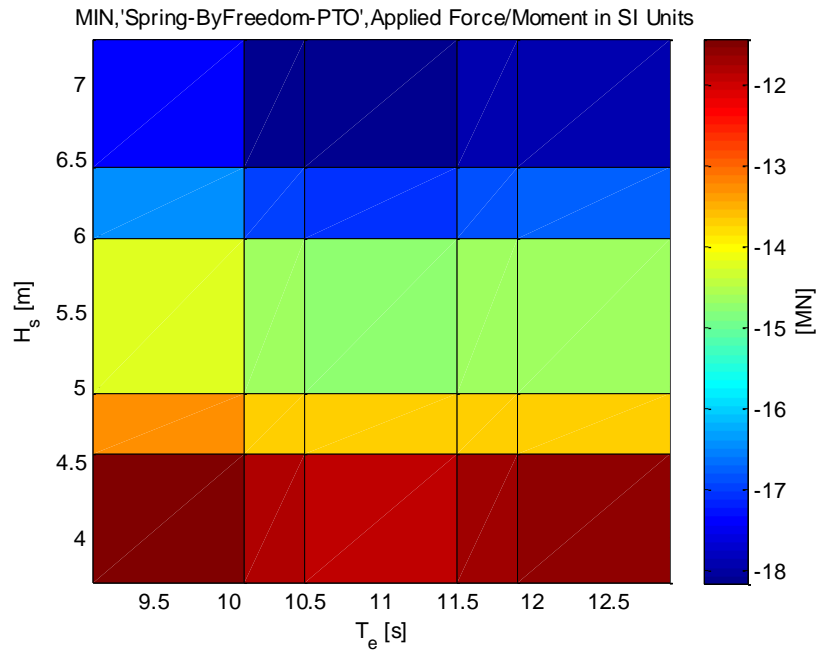
Figure 3-39 Min of PTO applied force for irregular unidirectional extreme waves
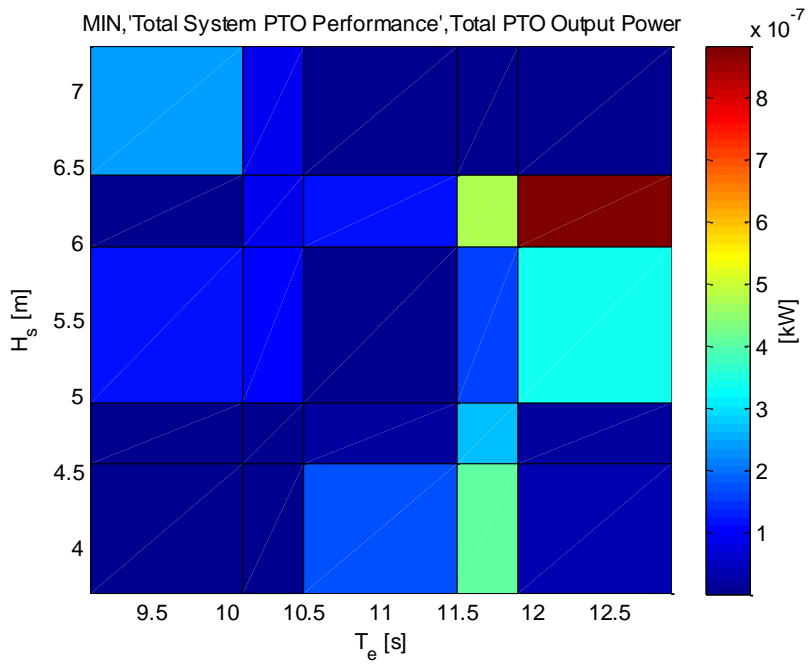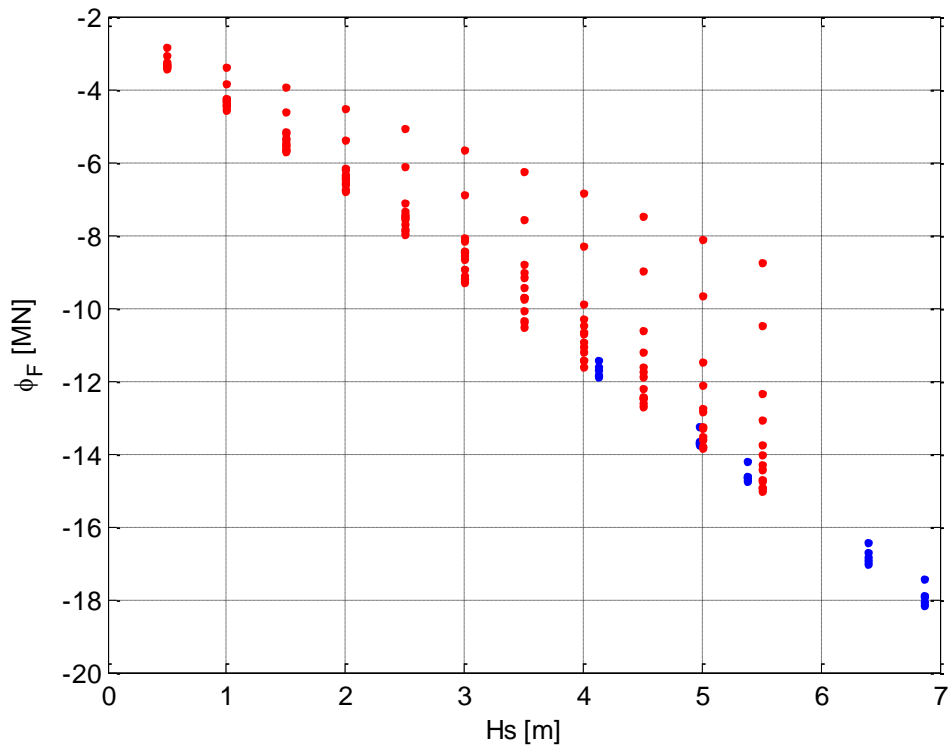

Figure 3-40 Min of PTO power output for irregular unidirectional extreme waves

Figure 3-41 Min of PTO applied force for unidirectional normal simulations (red) and unidirectional extremes (blue).

4 CONCLUSIONS

This report has investigated the motions, perfomance and PTO loads of a point absorber WEC where the float is a flat-circular plate. Numerical simulations of the device were run for normal and extreme environmental conditions based on site data.

The WEC model of the point absorber was based on a previous study /6/ and /7/. The mass of the float, pre-load tension and resonant frequency were maintained. However, modifications were made to the water level, PTO damping and the link lengths in order to optimise the performance of the WEC for the location.

The response and force amplitude operators showed that no resonant motions occurs in heave or in pitch. For long-period waves the surge motion exhibited nonlinear behaviour such as period doubling. The heave motions increased approximately linearly with respect to significant wave height. The motions of sway and surge during irregular spread waves was found to be large.

In previous studies, /7/, the PTO pre-load was set to prevent snatching loads. Simulations of unidirectional irregular waves revealed that the tether was no longer in tension for large wave height sea states. As equilibrium is required between the pre-load in the tether, the mass of the plate and the mean displaced mass of the plate, an increase in the pre-load would require a significant change to the draft of the flat-plate. To maintain consistency with previous results it was decided that the pre-load and the mean displaced mass should remain unchanged to avoid creating an incompatible data set with previous results.

Simulations of unidirectional and spread irregular waves has provided a significant range and volume of data for future numerical verficiation studies. The results of the simulations will be provided to the Customer for comparison to other simulation packages. The necessary tools to read the outputs have been provided as part of an earlier project /7/.

5 REFERENCES

/1/ Agreement for services and RCUH P.O #Z10027978, 15 April, 2013

/2/ Amendment No. 1 to the services agreement between the Research Corporation of the University of Hawaii and Garrad Hassan America, Inc, 14th August 2014

/3/ Email from Luis Vega to Jarett Goldsmith, 23th October 2015

/4/ Email from Luis Vega to Jarett Goldsmith, 31th July 2015

/5/ Email from Luis Vega to Jarett Goldsmith, 11th February 2016

/6/ Roadnight J, Child B, Mackay E. WEC Performance Model Verification – Progress Report #1. Hawaii National Marine Renewable Energy Centre – WEC Ocean Testing. 702053-UKBR-T-03-A. 29/01/16

/7/ Parkinson S, Child B, Buils Urbano R. WEC Testing Support – Progress Report #1. Hawaii National Marine Renewable Energy Centre - WEC Ocean Testing. 702053-UKBR-T-04-B. 11/04/2016

/8/ Michell JH, On the highest wave in water (1983). Phil. Mag., 36, 430-435.

/9/ Ewans, KC, Observations of the directional spectrum of fetch-limited waves (1998). Journal of Physical Oceanography. Vol. 23, page 495-512.

/10/ Hann M, Greaves D, Raby A, Snatch loading of a single taut moored floating wave energy converter due to focussed wave groups. Ocean Engineering 96 (2015) 258-271

/11/ Falcao, Wave energy utilization: A review of the technologies. Renewable and Sustainable Energy Reviews (2010), 14(3) pp 899-918.

APPENDIX A ENVIRONMENTAL CONDITIONS

The following sea states have been used in simulations of the WEC:

1. **Case I - Regular** sea states with wave amplitude a and wave period T defined using the following combinations have been simulated:

    a. Wave amplitudes a =0.4, 0.8, 1.2, 2, 3, 4 m

    b. Wave periods T = 1.58, 3.16, 4.74, 5.60, 5.7 6.32, and then every 0.316 s to 25.3 s.

    c. The (mean) direction of waves is along the x-axis ($MDIR = 0$).

    Only combinations of height and period that do not exceed the breaking wave steepness limit have been simulated. For deep water the wave breaking limit, given by the wave height to wave length ratio otherwise known as the wave steepness $\epsilon = H/L$, occurs at ϵ=1/7 /8/. The wave steepness for deep water waves can be written $\epsilon = 4\pi a/gT^2$ where g is the acceleration due to gravity.

2. **Case II - Unidirectional and irregular** sea states defined using the following range of significant wave height H_s=0.5,1.0,…,5.5 m and energy period T_e=5,6,…,17 s and the following additional specification:

    a. The frequency-dependent wave spectra (omnidirectional spectra) are described using a JONSWAP spectral shape with a peak enhancement factor γ=1. The JONSWAP spectral shape is given by:

    $$S_j(f) = \frac{\alpha g^2}{(2\pi)^4 f} \exp\left(-\frac{5}{4}\left(\frac{f_p}{f}\right)^4\right)\gamma^r \tag{8}$$

    $$r = \exp\left(-\frac{(f - f_p)^2}{2\sigma_j^2 f}\right) \tag{9}$$

    $$\sigma_j = \begin{cases} 0.07, & f < f_p \\ 0.09, & f \geq f_p \end{cases} \tag{10}$$

    where, f is the wave frequency, α is the energy scale, $f_p = 1/T_p$ is the peak frequency and σ_j is the peak-width parameter. The peak period T_p of the JONSWAP spectra is obtained using the fixed ratio between energy period and peak period $T_p = 1.17\, T_e$.

    It was decided that a JONSWAP spectrum would be used as a representation of the wave climate for each sea state. In this way, results from this study can be appllied to other sites (also assuming a JONSWAP spectral shape) by accounting for the site-specific distribution of wave height and period.

    b. The mean wave direction is along the x-axis, $MDIR = 0$.

    c. The same seed (initialising the random phases of wave components) was used for all simulations.

    d. The simulation duration was set at 3 hours. This duration is considered necessary to derive reliable estimates of extreme performance and load values.

3. **Case III - Directional spread and irregular** sea states defined as per case II and the following additional specification:

   a. Omnidirectional wave spectra were described using a JONSWAP spectral shape with a peak enhancement factor of $\gamma = 1$.

   b. The mean wave direction is along the x-axis, $MDIR = 0$.

   c. The directional distribution is described using a Ewans wind sea distribution /9/. The wave direction is denoted by θ. For unimodal sea states the direction distribution $D(\theta, f)$ is based on the wrapped normal distribution given by:

   $$D(\theta, f) = \frac{1}{\sigma(f)\sqrt{2\pi}} \sum_{k=-\infty}^{\infty} exp\left(-\frac{1}{2}\left(\frac{\theta - MDIR - 2\pi k}{\sigma(f)}\right)^2\right) \tag{11}$$

   $$\sigma = \begin{cases} 11.38 + 5.357\left(\frac{f}{f_p}\right)^{-7.929} & , \; f < f_p \\ 32.13 - 15.39\left(\frac{f}{f_p}\right)^{-2} & , \; f \geq f_p \end{cases} \tag{12}$$

   For the Ewans wind sea, the standard deviation is described empirically and is frequency dependent.
   Information regarding the directional spread of waves was not provided as part of this work. Equation (11) and (12) were applied as they provided a means of describing the directional distribution in the absence of other infomation. While the Ewans wind sea is theoretically specific to wind generated waves, a similar formulation can be used to describe swell waves using a different formula for σ. However, in DNV GL's experience, the Ewans wind sea representation of directional distribution offers a good description of directional spread for both wind and swell seas.

   d. The same seed (initialising the random phases of wave components) was used for all simulations.

   e. The simulation duration was set at 30 minutes. This duration is sufficient for deriving statistics of averaged quantities (mean power, etc.)

1. **Case IV – Extreme unidirectional and irregular** sea states defined using extreme return values for significant wave height. The values of H_s assocaited with the 1, 5, 10, 50 and 100 year return periods are given by H_s=4.13, 4.98, 5.38, 6.40 and 6.87 m respectively with mean associated energy period of T_e=9.6, 10.6, 11.0, 12.0, and 12.4 s. The following additional specification is defined:

   a. Omnidirectional wave spectra were described using a JONSWAP spectral shape with a peak enhancement factor of $\gamma = 1$ as given in Equation (8).

   b. The mean wave direction is along the x-axis, $MDIR = 0$.

   c. The same seed was used for all simulations.

   d. The simulation duration was set at 3 hours. This duration is considered necessary to derive reliable estimates of extreme performance and load values.

2. **Case V – Extreme directional spread and irregular** sea states defined using extreme return values for significant wave height with 1, 5, 10, 50 and 100 year return periods as defined in Case IV. The following additional specification is defined:

a. Omnidirectional wave spectra were described using a JONSWAP spectral shape with a peak enhancement factor of $\gamma=1$.

b. The mean wave direction is along the x-axis, $MDIR = 0.$

c. The directional distribution is described using a Ewans wind sea distribution as described in Equations (11) and (12).

d. The same seed (initialising the random phases of wave components) was used for all simulations.

The simulation duration was set to 30 minutes.

ABOUT DNV GL

Driven by our purpose of safeguarding life, property and the environment, DNV GL enables organizations to advance the safety and sustainability of their business. We provide classification and technical assurance along with software and independent expert advisory services to the maritime, oil and gas, and energy industries. We also provide certification services to customers across a wide range of industries. Operating in more than 100 countries, our 16,000 professionals are dedicated to helping our customers make the world safer, smarter and greener.